UNIVERSITY OF PAVIA
FACULTY OF ENGINEERING

UNIVERSITY SCHOOL OF ADVANCED STUDIES - IUSS PAVIA

Developing Fragility Curves for Existing Concrete Bridge in Naples (Italy) under Bi-Directional Seismic Loading Using Dynamic Nonlinear Time History Analyses

A Thesis Submitted in Partial Fulfilment of the Requirements
for the Degree of Master of Science (Laurea Magistrale) in

Civil Engineering for the Mitigation of Risk from Natural Hazards
Reduction of Seismic Risk (ROSE) Curriculum

by

Mohamed Hamad
Supervisors: Prof. Roberto Nascimbene, Dr. Davide Bellotti, Dr. Volkan Ozsarac

March 2026 a.a. 2023-2026

ABSTRACT

This thesis investigates the seismic fragility of a typical two-span reinforced concrete (RC) precast T-girder bridge located in Naples, Italy. The bridge, characterised by two 17-meter spans and two column bents connected by an inverted T-cap beam with double cantilevers, was analysed via a detailed 3D finite-element model in OpenSees v3.8.0 and validated against MIDAS Civil.

This study aims to offer essential insights into the seismic performance of the bridge across three representative configurations. It focuses on the interaction between precast girders and the cap beam under three cases: (i) fully fixed condition for the pier, and (ii-iii) partially fixed configurations arising from thin unreinforced elastomeric pad bearings between concrete surfaces, including the effect of 30° skew relative to the bridge's longitudinal

A non-linear time history analysis was performed for 90 synthetic earthquakes, utilising the curvature ductility ratio as the primary engineering demand parameter (EDP). Based on these simulations, different levels of performance and damage limit states were identified. The study used the results of the non-linear time history analysis to assess the behaviour of the structure during seismic events and to enhance the level of resilience of bridges that are structurally analogous to the studied bridge against potential damage patterns.

The results indicate that the implementation of elastomeric pad bearings markedly improves the bridge's seismic resilience. As peak ground acceleration (PGA) increases, the probability of failure for all bridge components rises across the three cases. The fixed-pier configuration is most vulnerable to pier failure, while the friction configurations experience initial failure in the bearings, then in the piers under high-intensity shaking. The cap beam is characterised by significantly higher median fragility intensities across all configurations, indicating that it is generally quite strong in the considered hazard range.

KEYWORDS: Highway roadway; Elastomeric pad bearings; double-column piers with inverted T-Cap-Beam; seismic fragility; Dynamic nonlinear time history analysis; Bi-directional Ground motions

ACKNOWLEDGEMENTS

First, I would like to express my deepest gratitude to Allah for granting me the ability to complete my master's thesis. Second, I would like to thank my research group with whom I worked on my master's thesis. I would like to express my deepest gratitude to my supervisor, Professor **Roberto Nascimbene**, for trusting me to work with him. I really appreciate his support in every possible way throughout this master's thesis. I would say that your friendliness, flexibility, and kindness have been truly inspiring, and I hope to be so throughout my life and career. I am also extremely grateful to my co-supervisor, Dr **Davide Bellotti**, for his support and for providing me with all the needed data, and for his immense patience in guiding me step-by-step through the modelling process with two software programs that were entirely new to me. My special thanks also to my co-supervisor, Professor **Volkan Ozsarac**, for his significant contributions, his constant willingness to help, and his incredibly fast support whenever I needed it. I really feel very lucky to work with you.

I would like to extend my special thanks to Professor Barbara Borzi, Head of the Risk Scenario Department at EUCENTRE, for her trust, support, and for welcoming me at the EUCENTRE office. Additionally, I am deeply grateful to Dr Antonino Famà for his support and guidance during my time at the office.

I would like to express my deepest gratitude to all the professors of the ROSE course. I am extremely impressed by their high teaching skills and unique ability to explain complex subjects with such clarity and simplicity. A special thanks to Professor Carlo G. Lai, Professor Guido Magenes, and Professor Ricardo Monteiro for conducting my interview and giving me the opportunity to participate in this distinguished program. I am grateful for all the knowledge and inspiration I have received from each of them.

I would like to thank my group of classmates. We fought together to overcome all difficulties during this intensive master's program. Thank you—Talha, Santiago, Vandwesen, Ali, Abdelhade, Luca, Baruja, and Maria—for your friendship and for everything. In addition, I would like to give special thanks to my senior, Elias Yacoub, for his guidance when I needed help over the past two years. Wish them all success throughout their career and life.

Words cannot express how grateful I am to my parents for their support throughout my life and to my brothers for their encouragement. I am thankful to my whole family, with special thanks to my uncles for their financial support. Finally, I dedicate my thesis to my wife and sons. Their love has given me the strength to accomplish this thesis.

TABLE OF CONTENTS

LIST OF FIGURES

LIST OF TABLES

1 INTRODUCTION

1.1 INTRODUCTION AND MOTIVATION

Bridge structures are the most vital "lifeline" elements required to transport goods and people efficiently. There are estimated to be approximately 120,000 to 180,000 road bridges in Italy alone. The total number of bridges in Italy's infrastructure system reflects the complexity and fragmentation of ownership within Italy's overall stock of bridges (Santarsiero et al., 2021).

Although Italy is in a seismically active region of the world, only a small percentage of the nation's database of bridge collapses or extreme damage is due to earthquake-induced forces. A study of 180 documented cases of bridge failures occurring in Italy over the past 30 years was conducted. In only two of these cases were earthquakes the primary cause of collapse (Scala et al., 2025). While it is rare for bridge failures to result in loss of life, they cause devastating economic impacts on the national economy. Typically, these impacts occur as a result of dual losses: direct cost of reconstruction, and indirect loss resulting from traffic disruptions (i.e. paralysis of the flow of traffic), and disruption of supply chains (which typically results in a loss at least five to ten times greater than the direct cost of reconstruction)—Morandi (2018) found that the ratio of indirect loss to direct loss in the case of the collapse of the Morandi Bridge was 8:1 (resulting in a loss of €9 billion + of regional GDP). Strategic link failures create network bottlenecks, severing emergency access and industrial corridors, establishing bridges as economic single points of failure (Lavezzo, 2022). This thesis utilises a Performance-Based Earthquake Engineering (PBEE) approach to establish fragility curves for a bridge to improve the ability of society in Naples, Italy, to withstand earthquakes. The use of dynamic nonlinear time-history analysis of bidirectional seismic loading will generate data through the undertaking of a PBEE study, which is intended to provide an accurate, risk-informed assessment to enable policymakers to prioritise retrofitting to protect infrastructure and regional economies from future earthquake damage.

1.2 RESEARCH OBJECTIVES

While many studies have examined straight or regular RC bridges, there has also been a growing focus on bridges with horizontal curvature, skewness, and irregularity, which demonstrate more complex load paths and increased seismic vulnerability (Song et al., 2024). Furthermore, most existing fragility models are developed for tectonic hazards without explicitly considering ground motions caused by volcanoes.

To address the practical problem and the identified gap, the thesis is structured around the following research questions:

i) How do the specific interactions between precast girders and cap beams across three configurations (fixed-pier, orthogonal friction, and 30° skewed friction) characterise the demand patterns and govern the damage limit states of the bridge?

ii) What are the characteristic seismic performance parameters (median intensity measures and dispersions) of each type when subjected to bidirectional synthetic volcanic ground motions?

Bridges located within the Naples area experience seismic activity associated with nearby volcanic sources (e.g., Vesuvius and Campi Flegrei), where the induced ground motions from these sources may exhibit significant differences from the tectonic record regarding to their frequency content, duration and shapes of the ground motions. The differences between the ground motions induced by nearby volcanic sources and the tectonic record significantly affect the behaviour and damage patterns of bridges. Actual earthquakes, including volcanic and near-fault events, exert forces in two horizontal directions simultaneously. Using only one direction does not accurately represent the real seismic demands on bridges (Feng et al., 2018). Developing fragility analysis through unidirectional approaches underestimates demands by 40-65% in skewed bridges (Noori et al., 2019a).

1.3 THESIS OUTLINE

The thesis is organised into six chapters to present a clear progression from motivation to methods, application, and decision-relevant findings.

Chapter 1: This chapter clarifies the motivation for assessing the seismic vulnerability of existing reinforced concrete bridges located in seismically active regions like Naples. The research focuses on outdated design practices and the lack

of fragility data regarding seismically induced volcanic hazards. Given this context, the goals and objectives of the research are defined, and the research questions are posed. Additionally, the study is framed within the context of Performance-Based Earthquake Engineering (PBEE), emphasising its relevance to infrastructure resilience and risk reduction.

Chapter 2: This chapter contains the seismic damage mechanism literature of reinforced concrete bridges, as well as the fragility curve development literature. The authors examine different types of methods that have been used to develop fragility curves, including Analytical, Empirical, Experimental and Hybrid Methods. They identify the uncertainty present in fragility assessments and the degree to which a structure is vulnerable. In addition, they provide an overview of the areas where there are still some gaps in the current body of knowledge.

Chapter 3: The chapter describes the characteristics of the Tangenziale di Napoli's chosen highway bridge, including geometry, structural form, and type of bearing system, as well as when it was built. An explanation of Naples' seismicity and its volcanic and tectonic origin, along with the classification and selection of synthetic ground motions caused by volcanism.

Chapter 4: This chapter aims to clarify the development of detailed three-dimensional finite element models using OpenSees software. It includes two main topics related to modelling steps (defining boundary conditions, element properties, and bearing properties) in three different bridge models and developing fragility curves (Damage state definitions, Engineering Demand Parameters (EDPs), and the analytical method for creating fragility curves)

Chapter 5: This chapter contains the nonlinear response of structures for global and each component, with verification against the MIDAS model. The cloud-based analysis produces probabilistic fragility curves for piers, bearings, and the bridge. In addition, an explanation of how the analytical results relate to the research purpose and previous literature on the influence of bearing performance on increased levels of seismic intensity is included.

Chapter 6: This chapter summarises key findings and draws evidence-based conclusions regarding the earthquake fragility of bridge types discussed in this research. It identifies key limitations of the present research and provides future directions for research, including alternative intensity measures, volcanic/tectonic combined hazard assessments, experimental calibration of unreinforced elastomeric bearings, and regional-scale fragile applications.

2 LITERATURE REVIEW - STATE OF THE ART

2.1 INTRODUCTION AND PROBLEM DESCRIPTION

2.1.1 Motivation

Reinforced concrete (RC) bridges are key elements of roadway networks, and their malfunction after earthquakes can severely disrupt mobility, emergency response and post-event recovery, and experience from recent earthquakes in Italy and worldwide has shown that damage or collapse of a limited number of bridge structures may isolate urban areas and critical facilities, emphasizing the need for rational tools to quantify bridge seismic vulnerability and to prioritize retrofit interventions (Borzi et al., 2015a; Choi et al., 2004). Girder beam Reinforced concrete bridges constitute a large component of the Italian road network and are essential for connectivity and emergency response during earthquakes. The destruction caused by earthquakes such as Friuli 1976, Irpinia 1980, L'Aquila 2009, Northridge 1994, Kobe 1995 and Tohoku 2011 have revealed how fragile reinforced concrete bridges can be, with typical damage including: the failure of columns under flexural shear forces, sliding or collapse of bearings, and deck pounding or collapse (Jeon et al., 2016). For specific bridge types, some studies have developed fragility curves using detailed 3D nonlinear models with non-linear time history analyses and it has been shown that (i) the most vulnerable elements are typically columns and bearings, (ii) boundary conditions at abutments (e.g., roller vs stiff participation) can greatly influence seismic response of the structure, and (iii) geometric irregularities and details (curvature, skew angle, column height, hinge distribution) may significantly alter component as well as system fragilities (Choi et al., 2004; Jeon et al., 2016; Ramanathan et al., 2015a). For Italian RC bridges, recent work has shown the feasibility and importance of automatic, nonlinear fragility assessment for large stocks, as well as the need for detailed, bridge-specific studies to accurately represent real configurations and details (Borzi et al., 2015a; Choi et al., 2004; Perdomo et al., 2022). Overall, fragility curves are used to measure, in probabilistic terms, the probability of different levels of damage at different earthquake intensities. It helps to make safer, more cost-effective and better prioritised decisions for the design, evaluation and retrofitting of concrete bridges.

2.1.2 Problem Description

Many structural systems that include concrete beam bridges have high seismic vulnerabilities. Most of the infrastructure from the 1960s and 1970s was built at times when there were no seismic design provisions for earthquake resistance, or they did not meet modern standards. The structural deficiencies are often found due to a lack of ductility or insufficiency of detailing in the flexural plastic hinge zone, which may lead to a significant likelihood of failure for most structures subjected to moderate to high levels of ground motion. There is a lack of site-specific and typology-specific fragility curves for existing RC beam bridges in Naples that integrate:

i) Realistic three-dimensional nonlinear modelling.
ii) Bi-directional artificial volcanic ground motions.
iii) Curvature-based damage states.

Beam bridges are the simplest and most common type of bridge used in highway projects because they are efficient and easy to construct. They are supported by abutments and, if necessary, intermediate piers, and are typically used for short- to medium-span structures. For spans less than about 20 meters, the deck is usually made of a reinforced concrete slab, while composite systems with reinforced concrete slabs supported by prestressed girders are popular for spans up to around 45 meters.

The connection between the superstructure and substructure in beam bridges is non-monolithic, constructed using bearings that permit controlled movement and force transfer. Beam bridges can be configured as single- or multi-span systems, with bearings placed at supports or within spans as expansion joints. Piers are typically constructed of reinforced concrete and can have solid circular or rectangular cross-sections.

The bridge investigated in this thesis is an overpass beam bridge with two spans, each span is 17 m. It has composite decks consisting of reinforced concrete slabs and prestressed girders, and a reinforced concrete pier with a solid rectangular

section. The seismic vulnerabilities of this structure, as evidenced by damage observed in past earthquakes, are discussed in the following section.

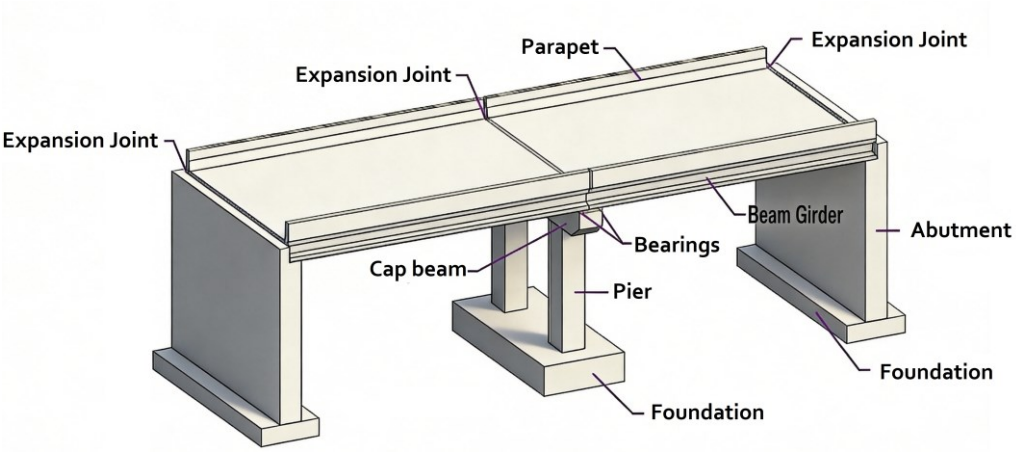

Figure 2-1 Typical overpass bridge components

2.2 SEISMIC DAMAGE TO REINFORCED CONCRETE BRIDGES

Bridges are susceptible to damage under earthquake excitation; severe structural damage has occurred in the recent past and on a global basis in several such earthquakes. The reconnaissance and analytical studies throughout the world after earthquakes have observed a consistent pattern of damage in bridges, which falls into six broad categories (Chen & Duan; *Priestley et al, 1996*):

- Pounding and unseating of the deck
- Bearing failures
- Foundation-related problems
- Shear and flexural failures of piers
- Cap-beam and joint damage
- Abutment damage

These damage mechanisms are generally associated with factors such as typology of the structure, age at construction, details in design practice, soil-structure interaction and ground motion properties (Priestley et al, 1996). The 1999 magnitude 7.3 Chi-Chi earthquake caused extensive damage to infrastructure in central Taiwan, and demonstrated how highway bridges become susceptible to surface failure, leading to massive deck displacements and pier failures, thus demonstrating the need for better seismic design practices. The research assessed nearly 1,000 highway bridges spanning the regions of Taichung and Nantou, and Changhua and Yunlin counties (Chang et al.). SEE Figure 2-2.

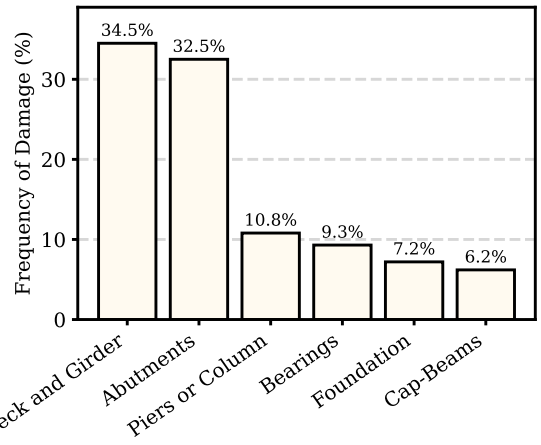

Figure 2-2 Statistics of Bridge Damage due to Chi-Chi earthquake

2.2.1 Pounding and Unseating of the Deck

Expansion joints reduce stresses in superstructures arising from temperature-dependent volumetric changes in concrete over time. However, damage to bridges due to pounding at their expansion joints has been widely observed in almost all the severe earthquakes in the past several decades. When the relative movement of nearby bridge girders is greater than the gap size, girder pounding takes place. Pounding can lead to girder collapse in addition to cracking concrete or crushing steel reinforcement. Because of this, the pounding is the most frequent cause of bridge damage among a number of factors (Chen & Duan). While unseating girders during earthquakes is less frequent than pounding, it has disastrous effects on human life and often results in catastrophic consequences. The reconnaissance report on the 2008 China Wenchuan Earthquake indicates that the primary reason for girder dislodgement is insufficient seating lengths of the girders (Lin et al., 2010). SEE Figure 2-3.

(a) (b)

Figure 2-3 (a) Pounding of a bridge, and (b) Unseating of girder in the 1999 Chi- Chi Earthquake, Taiwan, gathered from (Moehle et al., 2000)

(c) (d) (e)

Figure 2-4 Santa Clara River Bridge pounding damage in the 1994 Northridge earthquake. (c) Barrier railpounding damage; (d) abutment pounding damage; (e)Unseeting 1971 San Fernando earthquake (sample span, due to bridge skew.

The seismic behaviour of the bridge deck is dependent upon both the dynamic characteristics of the bridge girders and various other forces (e.g., due to changes in ground motion, impacts between spans, and local soil conditions). Because of the variation in vibration characteristics along a long span bridge having numerous piers, a single base excitation cannot represent the variability in seismic wave velocity or soil profile at each pier, which can lead to a nonuniform forcing function resulting in asynchronous vibrations between adjacent spans. The resulting is a relative displacements can generate pounding at the expansion joints (Chouw & Hao, 2005). Moreover, Several experimental, analytical and review studies confirm that the impact of pounding creates duration, high-intensity acceleration peaks in colliding structures, which can increase relative displacements between the spans. This required increasing the seat width (Lin et al., 2010).

2.2.2 Shear and Flexural Failures of Piers

The failures of piers due to shear and flexure constitute one of the most critical damage mechanisms in bridge structures, as piers serve as the primary components of the gravity and lateral force-resisting system. During strong earthquakes, a large number of highway bridges have experienced severe damage/collapse due to inadequate flexural-shear strength and ductility of the bridge piers in the recent earthquakes (*Priestley et al, 1996*), like the 1995 Kobe Earthquake, the 1989 Loma Prieta Earthquake, the 1987 Whittier Earthquake, and the 1971 San Fernando Earthquake. SEE Figure 2-5, and Figure 2-6.

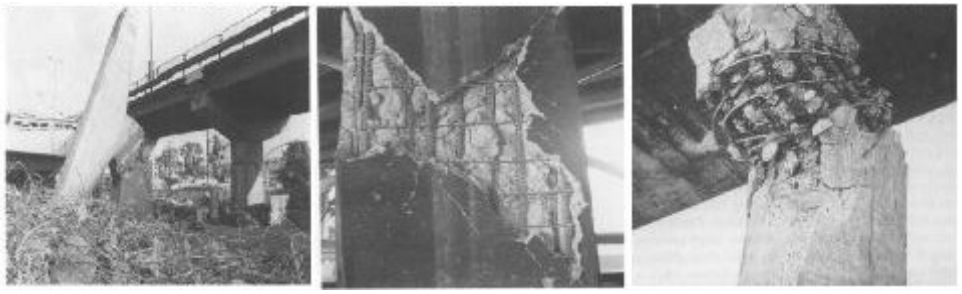

(a) (b) (c)

Figure 2-5 A few damages scenario of a few highway bridges in the recent; (a) Pier flexural-shear failure at midheight of Route 43/2 overpass, due to premature termination of longitudinal reinforcement in the 1995 Kobe earthquak, (b) Brittle shear failure of column of the I-5/I605 seperator, 1987 Whittier earthquake, (c) Shear failure within plastic hinge region, 1971 San Fernando earthquake

(d) (e) (f)

Figure 2-6 A few damages scenario of a few highway bridges in the recent earthquakes; (d) Bond failure of lap slices of bridge pier in the Loma Prieta earthquake in 1989, (e) Flexural failure of a bridge pier in the 1995 Kobe earthquake, (f)) Flexural failure above pier base of piers of the Hanshin Expressway in the 1995 Kobe earthquake

In line with this, the 2008 Wenchuan earthquake revealed that shear–flexural failure of reinforced concrete (RC) piers was among the most prevalent and critical damage modes. Common observations included concrete cover spalling, diagonal

cracking, buckling and fracture of longitudinal reinforcement, and loss of load-carrying capacity, particularly in single-column piers and bridges with insufficient transverse reinforcement (Han et al., 2009).

Curved, skewed, and irregular bridges, RC piers may experience significant flexure–torsion interaction, leading to altered damage patterns, upward migration of plastic hinges, and reduced flexural and torsional capacity compared to uniaxial loading condition, and During the 2008 Wenchuan earthquake in China, bridge piers of skewed and curved bridges sustained significant damage (P. Wang et al., 2014).

The Northridge earthquake caused the collapse of seven concrete freeway bridges. The failure of six out of the seven bridge structures that failed in the 1994 Northridge earthquake has been attributed to column shear failures due to the failure of transverse reinforcement. Column shear failures often lead to a loss of structural integrity, resulting in failure under gravity loads (Priestley et al, 1996).

2.2.3 Bearing Failures

Seismic failures of bridge bearings often appear as slippage, displacement, or significant shear deformation during intense ground shaking. Although bearings can protect bridge piers by acting as fuses to reduce seismic loads on the substructure, they frequently cause issues due to underestimating relative displacements and having insufficient restraining force capacity, such as separation of expansion joints, deck settlements, or even complete settlement of girders (Lu et al., 2011).

(a) *(b)* *(c)*

Figure 2-7 A few damage scenarios during the 1990 Chi-Chi earthquake; (a) Sliding/friction mechanism of bearing, Don-Fong bridge; (b) Sliding/friction mechanism of bearing, Yen-Fen bridge; (c) Many rubber bearings slide away

The Tohoku earthquake of 2011 provided more evidence that large relative displacements and long-duration shaking can lead to the total failure of bearing systems on modern-day bridges. Therefore, when designing bridges for seismic events, engineers must ensure that they have sufficient lateral and vertical

displacement allowance, that their structural elements have proper anchorage systems, and that the engineer considers nonlinear bearing behaviour in accordance with the demands of a given site (Scawthorn & Porter, 2011).

2.2.4 Abutment Damage

Abutments have been repeatedly identified as vulnerable components, particularly in bridges founded on soft soils or poorly compacted abutment backfill, where Seismic failures of abutments are classified as slumping and rotation. Under longitudinal excitation, active earth pressures increase, while deck-backwall pounding generates extreme passive pressures, pushing the abutment base inward with mobile soil, while the superstructure restrains upper movement (*Priestley et al, 1996*).

(a) (b)

Figure 2-8 Two failure scenarios for the abutments: (a) due to slumping and rotation failure, Rio Banano bridge, 1990 Costa; (b) due to passive pressure, Rio Viscaya bridge,1990 Costa

Most of these failures can be attributed to the increasing dynamic soil pressure against the abutments, due in part to vertical ground accelerations and to passive pressure due to bridge deck pounding against the back wall. Bridge deck pounding can produce large amounts of shear cracking within the side walls, and in cases where the length of the bearing seat is insufficient, it can result in the unseating of bridge spans (Di Sarno et al., 2019; Han et al., 2009). Furthermore, Geotechnical factors also contribute significantly to failure; for example, seismic-induced infill settlement and inadequate lateral confinement of backfill materials can result in visible cracking and subsidence of roadways (Di Sarno et al., 2019).

The most extreme cases of abutment wall failure may occur due to slope instability, soil liquefaction, or displacement of ground faults on the surface, causing entire

abutments to tilt or shift transversely, resulting in total complete loss of superstructure support (Kawashima et al., 2009).

2.2.5 Cap beam Joint Damage

Cap beams are critical components in transferring seismic loads from the superstructure to supporting structural members or columns. Cap beam failures are rarely a critical design issue unless they result directly from design constraints imposed by the weight of the structure above. The 2008 Wenchuan earthquake demonstrated that seismic shear failures of bridge cap beams resulted from insufficient shear reinforcement and poor detailing of anchored connections between the cap beam and the column. The seismic shear failures occurred primarily at locations where the cap beam connected to a single-column pier or where the cap beam supported a large amount of weight and thus had difficulty carrying the seismic loading imposed on it (Han et al., 2009). As further evidence, joint shear failures have recently been identified as one of the most common reasons why the Cypress Viaduct collapsed, although almost no joint shear reinforcing has been used to address the high horizontal and vertical shear forces that are transferred across the connections. This lack of joint shear reinforcement has resulted in diagonal cracking in the joint regions, a common flaw contributing to the failures of double-deck viaducts, single-level multicolumn bents, and outrigger bent knee joints during the San Fernando and Loma Prieta earthquakes (Priestley et al, 1994). SEE Figure 2-9.

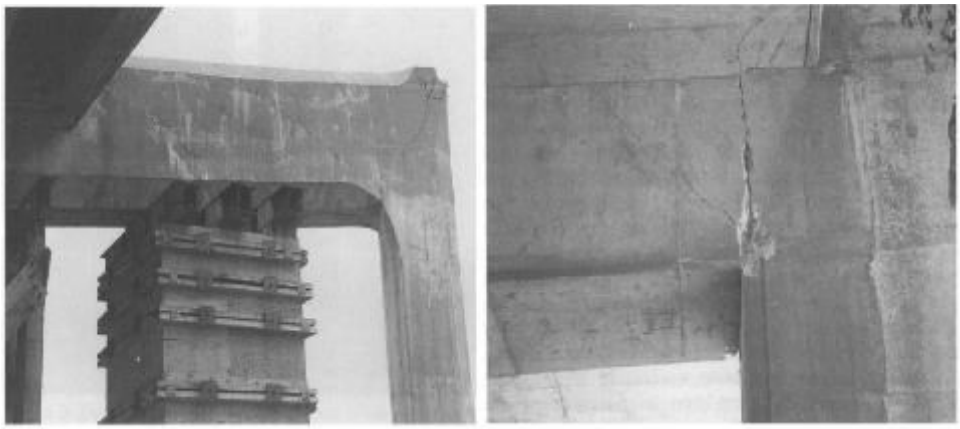

(a) (b)

Figure 2-9 Cap beam failure due to the 1989 Loma Prieta earthquake: (a) flexure and shear and joint failures, I-280 China Basin vidact, (b) Cap beam positive moment cracks at inner column face.

Following the 2016 Kaikōura earthquake, similar observations were made on cap beam damage and pier plastic hinging. These observations also highlight the close link between the substructure components under earthquake loading (Sarkis et al., 2018). For irregular bridge configurations, such as curved and skewed bridges, due to eccentric mass distribution and multidirectional ground motion, the girders also experience additional torque loading. Experimental and analytical work has demonstrated that these two force types will substantially reduce the effective shear and bending capacities of the beams; alter crack pattern; and accelerate the rate of damage if they are not considered in the design of the girders (P. Wang et al., 2014).

2.3 An Overview of Fragility Curve Development

Fragility curves show the probability that a structure will reach or exceed a certain damage state given a specific earthquake intensity measure (IM). Methods for developing fragility curves have been divided into five different types of methodologies: Expert-based, Experimental, Empirical, Analytical and Hybrid Methodologies. These methodologies differ from each other based on their need for data, computation and uncertainty (Lallemant et al., 2015a; Thakkar et al., 2023). In the last three decades, there has been a significant advancement in the development of bridge fragility curves. The first development of fragility curves was developed using probabilistic methods in the 1980s, whereas the latest methodologies are currently being utilised in the 2020s.

2.3.1 Expert-Based Fragility Assessment Method

The Expert judgment-based fragility is one of the oldest and simplest approaches. It depends on professional judgment and expert opinion when physical damage data is limited. Experts estimate damage probabilities for different hazard intensities based on experience, observed performance, or simplified modelling. The process typically involves surveying a panel of specialists via questionnaires to estimate damage distributions for various ground motion intensities, which are then compiled into damage probability matrices (Lallemant et al., 2015a; Muntasir Billah & Shahria Alam, 2015). The uncertainty associated with subjective assessments is treated using probabilistic frameworks, such as Bayesian belief networks, which quantify dependencies among bridge parameters, site conditions, and performance states (Franchin et al., 2016). By consistently combining expert opinions and visual inspection data for reinforced concrete (RC) girder bridges, (Franchin et al., 2016) showed how Bayesian belief networks can produce fragility estimates that can be used to prioritise retrofit actions at the network scale.

Expert-based techniques have the potential to be implemented rapidly and require limited data compared to other techniques, which can help with screening at the regional scale if an analytical model cannot be developed (Argyroudis et al., 2018).

However, there are still reliability concerns as results will heavily rely upon the experience level and number of experts on the panel. In order to address some of these limitations, many use Bayesian techniques such as updating prior distributions with additional empirical or experimental data to further refine their expert-based prior distributions (Lallemant et al., 2015a; Muntasir Billah & Shahria Alam, 2015). To enhance reliability, expert-derived curves are frequently used as priors in Bayesian updating frameworks that include analytical or observational data (Franchin et al., 2016; Tekeste et al., 2023).

2.3.2 Experimental Methods

Fragility curves of the experimental methods are conducted by direct observations on the performance of a structure using laboratory tests (cyclic loading or shaking table testing). Tekeste used a Bayesian updating methodology to create an integrated analytical model for the fragility of RC bridge components that combines sequentially collected shaking table test data with their results. Fragility parameters, expressed as the median and logarithmic standard deviation of intensity measures at failure, are updated using Markov Chain Monte Carlo (MCMC) sampling to integrate experimental evidence with prior analytical predictions. The adopted damage state definitions are based on standardised frameworks such as HAZUS or strain-based criteria, while cumulative lognormal functions are used to represent the probability of exceedance (Tekeste et al., 2023).

Experimental methods are characterised by their physical consistency and ability to capture complex nonlinear behaviour under controlled boundary conditions (Zhang et al., 2016).

Nevertheless, their use in full-scale bridges is limited by cost, size effects, and limited specimen availability. Tekeste et al. emphasised that small experimental datasets introduce high sampling uncertainty in Bayesian updating, especially when the prior distribution is weakly informative. Despite these limitations, experimental data are still important for model calibration and validation in analytical and hybrid fragile frameworks (Tekeste et al., 2023).

2.3.3 Empirical Methods

Empirical fragility analysis develops probabilistic relationships directly from post-earthquake damage observations linked to recorded or estimated seismic intensity parameters. The empirical framework involves classifying observed bridge damage into distinct limit states and fitting fragility functions using lognormal or ordinal regression methods (Buratti et al., 2017; Lallemant et al., 2015b). In a study employing Bayesian regression, Lallemant and co-authors fit empirical fragility curves for precast reinforced concrete structures. These curves were fitted using the damage survey data from the 2012 Emilia earthquake and the ground motions recorded from Shake Maps as predictor variables. Further, another empirical approach by Lallemant et al. used generalised linear models (GLM) and cumulative link models to quantify the uncertainty associated with damage-state transitions, as well as to account for the nonlinear nature of those transitions.

The advantage of empirical approaches in fitting fragility curves lies in their ability to be empirically-based; hence, they rely on actual data and include the unique regional construction practices and ageing characteristics that are typically difficult to quantify through an analytical approach (Karamlou & Bocchini, 2015).

However, the accuracy of empirically determined fragility values is heavily dependent upon the completeness and representativeness of post-event databases, which are frequently affected by poor instrumentation, incomplete reporting, and lack of uniform spatial coverage. The statistical dependency that exists among observed values may also introduce biases into fragility estimation if this relationship is not properly modelled. As such, empirical methods are most successful when used in conjunction with either analytical or Bayesian approaches to correct for both sampling and epistemic uncertainty (Straub & Der Kiureghian, 2008).

2.3.4 Analytical-Methods

Analytical methods dominate the literature, employing techniques such as Analytical Static Methods and Analytical Dynamic Methods. The primary advantage lies in their applicability when empirical damage data is unavailable, and their capacity to manage complex and highly non-linear structural behaviour (Silva et al., 2019).

However, technical limitations include computational demands that require extensive nonlinear time-history analysis, uncertainty in predicting seismic

response due to parameter variability, and potential accuracy issues when applying methods to different bridge types or regions (C. S. Yang et al., 2009).

2.3.4.1 Static Methods

Analytical static or mechanics-based methods for bridge fragility evaluation employ nonlinear static pushover analyses to estimate structural capacity under increasing lateral load patterns. The process involves creating capacity curves that relate base shear to displacement and then intersecting them with seismic demand spectra to determine performance points corresponding to predefined limit states (Contiguglia et al., 2022). Fragility functions are formulated using a lognormal cumulative distribution, where the probability of exceeding a specific damage state (DS_i) for an intensity measure (IM) is defined as:

$$P[DS_i|IM] = \Phi\left(\frac{\ln\left(\frac{IM}{\theta}\right)}{\beta}\right) \tag{2-1}$$

with (θ) and (β) denoting the median and logarithmic standard deviation of the fragility function, respectively (Altieri & Patelli, 2020). Methods such as the Capacity Spectrum Method (CSM), N2 Method, and Modal Pushover Analysis (MPA) have been widely utilised for bridge typologies with regular configurations (Contiguglia et al., 2022).

Static analytical approaches are beneficial because they require less computational effort and can explicitly model nonlinear response mechanisms through deterministic load–displacement relationships (Satyanarayana et al., 2025).

However, their inability to accurately capture cyclic degradation, higher-mode effects, and dynamic load redistribution limits their reliability in complex bridge systems. It is emphasised that such simplifications can lead to underestimating failure probabilities compared to fragility results based on dynamic analysis (Contiguglia et al., 2022).

2.3.4.2 Dynamic Methods

Analytical dynamic methods are simulation-based techniques that utilise nonlinear dynamic analyses to develop fragility curves by linking seismic intensity measures (IMs) with engineering demand parameters (EDPs). These methods include Cloud Analysis, Multiple Stripe Analysis, Incremental Dynamic Analysis, Analytical – Machine Learning, and Endurance Time approaches (Muntasir Billah & Shahria Alam, 2015).

Cloud analysis develops probabilistic seismic demand models (PSDMs) by correlating engineering demand parameters (EDPs) to intensity measures (IMs) based on unscaled nonlinear time-history analyses. Usually, the logarithmic regression model is typically expressed as:

$$\ln(EDP) = a + b\ln(IM) + \varepsilon \quad (2\text{-}2)$$

where (a), and (b) are regression coefficients and (ε) represents the residual variability (Lyu et al., 2024). The resulting (EDP, IM) pairs are fitted via log-linear regression in log-space, yielding a Probabilistic Seismic Demand Model (PSDM). The intersection of demand and capacity distributions (both modelled as lognormal) produces the fragility function (Satyanarayana et al., 2025). Cloud analysis has become a popular alternative for its relatively simple and computationally efficient nature, as it does not require record scaling of motion like IDA.

However, cloud analysis is limited by assumptions made within traditional cloud analysis. These assumptions include: (i) Responses are distributed according to a lognormal distribution. (ii) There exists a linear relationship between intensity measures and engineering demand parameters (Lyu et al., 2024; Pang et al., 2023; Zhuang & Pang, 2021). To address the limitations of cloud analysis, three new methodologies have been developed to improve the accuracy and efficiency of cloud-based assessments.

Enhanced Cloud Method (E-Cloud) was proposed in 2021, which aims to improve the stability of the logarithmic linear regression used in traditional Cloud analysis. The core of the E-Cloud method is the utilisation of the "intensifying" duration of as-recorded ground motions—the period before the motion reaches its maximum intensity. By extracting multiple "potential Cloud points" from this duration to supplement the peak response data, the E-Cloud method can produce stable and accurate fragility curves with significantly fewer ground motions than traditional methods, often requiring as few as 12 to 24 simulations (Zhuang & Pang, 2021).

In 2023, the Efficient and Accurate Fragility (EAF) method was introduced to deliver high-fidelity results of IDA and MSA while maintaining the low computational demand of Cloud analysis. Like E-Cloud, the EAF approach utilises the increasing duration of ground motions but employs them to generate transferred EDP-IM curves that replace traditional IDA curves. By recognising "L-Cloud" data records where the structural response exceeds a limit state—and

applying vertical statistics to these extracted curves—the EAF method avoids potential inaccuracies of Cloud regression models, providing a reliable solution for complex structures such as cable-stayed bridges (Pang et al., 2023).

In 2024, the Full Probabilistic Cloud Analysis via M-PDEM introduced a new way to do seismic structural analysis using an entirely new, physics-based probabilistic framework. This is different from previous approaches that required either empirical data fitting or use of lognormal distributions and linear correlations. The authors used the multi-probability-density-evolution method (M-PDEM), to find the transient probability density functions of the seismic-structural system by solving one-dimensional Li-Chen equations. This technique offers a highly accurate joint probability distribution of IM and EDP, particularly excelling in estimating low-probability "tail" events where traditional statistical models often fall short (Lyu et al., 2024).

Incremental Dynamic Analysis (IDA) is a predominant approach to the performance-based earthquake engineering of bridges. IDA is a method that involves a collection of ground motions that will be progressively scaled. Nonlinear time-history analyses will then be performed to trace the bridge response from elastic behaviour to significant damage or collapse. Detailed three-dimensional analytical models and non-linear time history analyses of typical highway bridge designs have been developed as a means of generating such analytical fragility curves, with the inclusion of the effects of multiple components (e.g. Columns, Bearings, Abutments) working together (Contiguglia et al., 2022; Nielson & DesRoches, 2007a).

IDA offers several critical benefits, such as high accuracy in capturing nonlinear system behaviour, and enabling precise calculation of parameters of fragility curves (median and dispersion) for each fragility damage curve (Nielson & DesRoches, 2007a; Satyanarayana et al., 2025). The approach can be with automated frameworks, which allow assessments of large national stocks for a specific type of bridge (Borzi et al., 2015b). Ramanathan's research shows that the Time History foundation by IDA enables comparisons across design eras based on performance deteriorations from seismic activity. It can address complex fragility issues, such as aftershocks. Bridges are categorised by Design Era or Seismic Detailing (before or after code change), with separate Fragility Curves for each to quantify how Modern Capacity Design reduces failure probability (Ramanathan et al., 2015b).

However, A key challenge with the use of IDA is its computational burden when performing multiple nonlinear analyses on a regional scale (Contiguglia et al., 2022). Besides high computational demands, IDAs may also be limited by using an intensity-based measure like PGA, which might not effectively assess the seismic performance of a multiclass system (Borzi et al., 2015b). Furthermore, the availability of geometric, material and soil properties data needs to be provided (Kheirkhahan et al., 2025), alongside the challenge of classifying bridges into appropriate subclasses, which is another issue that has limited the availability and accuracy of risk assessments at a regional scale (Mangalathu et al., 2016).

Multiple Stripe Analysis (MSA) combines Incremental Dynamic Analysis's accuracy with Cloud Analysis's efficiency to assess a structure's seismic fragility efficiently under controlled hazard levels and within probabilistic frameworks. For example, MSA analyses structures for how they respond under different levels of peak ground acceleration based on unique sets of ground motions assigned to each of the IM levels, as opposed to using the same set of ground motions repeatedly while trying to minimise unnecessary scaling. At various intensity "stripes," the calculations of the demands placed on a structure are compared with capacity thresholds, which allows us to find the likelihood of a structure's exceeding the limit states of either damage or collapse. With the establishment of each discrete probability point, we can find and fit a multivariate lognormal cumulative distribution function that corresponds to the fragility curve we calculate at the conclusion of the MSA process (Borzi et al., 2015b).

Some of the key advantages of Multiple Stripe Analysis are that the technique offers a high degree of accuracy and stability in terms of fragility estimation due to de-aggregation of the hazard, and that scaling of ground motion is minimised compared to the Incremental Dynamic Analysis technique (Borzi et al., 2015b).

However, MSA is computationally intensive due to the need to perform many nonlinear dynamic analysis tasks, particularly when dealing with complex geometries in bridges. include its continued dependence on the lognormal distribution assumption, its tendency to result in fixed intensity stripes that focus on the “left tail” of collapse fragility, and its potential to be inadequate in dealing with structures that have a plan extension and thus many important vibration modes, as in the case of peak ground acceleration (Borzi et al., 2015b). There is also a possibility that a small number of stripes may result in biased fragility, and that simplified models may be inadequate in representing failure mechanisms (Shabani & Kioumarsi, 2023).

2.3.5 Hybrid Methods

Hybrid fragility methods are a sophisticated approach to decreasing uncertainty regarding seismic vulnerability assessment. They accomplish this task by using an integration of analytical approaches (static or dynamic), experimental and empirical evidence to compute a probabilistic update scheme for estimating seismic vulnerability when pure methods are limited. They aim to give more realistic, yet still practical, estimates of damage probabilities. Hybrid techniques utilise a Bayesian approach for updating analytically generated fragility curves based on incremental dynamic analysis from experimental data through the use of a Markov Chain Monte Carlo (MCMC) sampling method to generate statistically consistent posterior fragility functions with low dispersion (Tekeste et al., 2023).A new hybrid approach was developed by (Fu et al., 2024) using a Bayesian Network integrates data from finite element analysis and damage assessment for Infrastructure Systems to create System-Level Fragility curves to increase reliability in the seismic assessment through using complementary data sources and better characterising structural behaviour probabilistically.

A 2024 study on RC continuous bridges near faults combines Incremental Dynamic Analysis (IDA) to obtain yield displacement with pushover analysis (POA) to obtain ultimate displacement, then builds fragility curves from both capacities (Htay et al., 2024). The limitation of this approach is that it depends on high-quality non-linear models: accurate representation of confined concrete, cyclic steel, plastic hinge construction and pier-superstructure interactions is required; Otherwise, fragility curves can be misleading. This requires consistent use of yields and final displacements from two different analyses (IDA and POA) in the same probability framework, which can create uncertainty in defining damage state thresholds (Htay et al., 2024).

2.3.6 Damage characterisation

This section outlines the approach for calculating direct physical damage to bridges. To determine the fragility functions that describe the conditional probability of exceeding a damage state for the entire bridge, damage must be characterised at the structural level. Damage can be characterised either at the structure level (based on global structural response) or at the component level (using component-specific damage models). Frameworks like (Hazus Earthquake Model Technical Manual), SEE Table 2-1, which link Engineering Demand Parameters (EDP) to damage limit states (DLS), offer standardised damage state definitions for bridges at the structural level. There are five damage states defined for highway system components. These include None, Slight, Moderate, Extensive,

and Complete. The functionality of a component is determined by its damage state probability (immediately post-earthquake) and the percentage of expected functionality after a given time. Provide uniform definitions of structural damage states for bridges according to Nielson, The most critical component (pier, cap beams, bearing, abutment, etc.) can be generated by statistically combining component fragility curves using reliability theory tools, or by using reliability theory tools to create a system-critical component (Nielson & DesRoches, 2007b).

Table 2-1 Definition of damage states

Damage Limit State	Definitions
None (DLS-0)	No bridge damage
Slight/Minor (DLS-1)	Minor cracking and spalling on the abutment, cracks in shear keys at abutments, minor spalling and cracks at hinges, minor spalling at the column (damage requires only cosmetic repair), or minor cracking to the deck.
Moderate (DLS-2)	Any column exhibiting moderate shear cracks and spalling (while remaining structurally sound), moderate movement of the abutment (<2"), extensive cracking and spalling of shear keys, connections with cracked shear keys or bent bolts, keeper bar failure without dislocation, rocker bearing failure, or moderate settlement of the approach.
Extensive (DLS-3)	Any column failure without collapse - shear failure — indicating the column is structurally unsafe, significant residual movement at connections, major settlement approach, vertical offset of the abutment, differential settlement at connections, or shear key failure at abutments.
Complete (DLS-4)	Any column collapsing and connection losing all bearing support could lead to imminent deck collapse and tilting of the substructure due to foundation failure.

2.4 Uncertainty in Developing Fragility Curves for Bridges

The construction of seismic fragility curves for bridges contains uncertainty due to the unpredictable behaviour of earthquakes, the variability of a structure's response to shaking, and the uncertainty due to restrictions on the data and assumptions used in constructing the models. Each of these uncertainties affects the accuracy of vulnerability estimates to the extent that they affect the reliability of the seismic risk estimates. In many cases, ignoring uncertainty results in

estimates of fragility that are either too optimistic or too conservative, resulting in an inaccurate estimate of the reliability of the bridge systems. The inaccuracy of static fragility estimates for deteriorating bridges is also caused by other time-dependent uncertainties, of which corrosion is a significant contributor (Bhandari, 2023).

2.4.1 Aleatory Uncertainty (Record-to-Record Variability)

Aleatory uncertainty is caused by the unpredictable nature of ground motions, and variability in ground motion's intensity measures, and frequency are examples of record-to-record uncertainty because they cause variations between records from the same source that have the same or similar magnitudes (Gardoni et al., 2003; Wu et al., 2021).

2.4.2 Epistemic Uncertainty (Knowledge-Based)

It arises from limited knowledge about material strength and geometric properties, corrosion evolution, boundary conditions across bridges, and the design era (older vs. modern), all of which significantly influence seismic fragility and its time dependence (Choe et al., 2009; Ramanathan et al., 2015c; Nielson & DesRoches, 2007).

Uncertainty regarding capacity/demand models: It has been shown that Probabilistic Seismic Demand Models (PSDM) are affected by errors in regression fitting, as well as by the choice of intensity measures and the calibration of capacity thresholds. Errors in these models have a significant effect on the fragility parameters (median θ & dispersion β) of an infrastructure item (H. Z. Yang & Koh, 2021). Finite element representations of these parameters, as well as assumptions regarding hysteretic behaviour and soil-structure interaction (SSI), such as the near-surface soil properties, greatly affect the seismic demands and fragility of an infrastructure's foundations, abutments, bearings and unseating, and can cause a significant difference between analytical prediction and actual performance (Xie & DesRoches, 2019).

During much of the past few decades, researchers have assumed that the soil surrounding a bridge structure is a fixed base. Current research suggests that this assumption is not always correct, especially when considering the soil-structure interaction (SSI) in the seismic performance of bridges. Fixed-base models do not consider the flexibility and energy dissipation of the soil/foundation system. While these assumptions can often be used to produce reliable screening-level or regional-level fragility studies (Li et al., 2020; Stefanidou & Kappos, 2019; Zhao et al., 2021).

They may not be as appropriate for use on sites with soft or liquefiable soils undergoing some type of scour, with deep or pile foundations, or under conditions of near-fault seismic motion. In these latter cases, SSI can have a significant effect on the period, damping, and force versus deformation demands of a structure, resulting in the fixed-base assumption being an inappropriate approach (Forcellini & Alzabeebee, 2023; Li et al., 2020; X. Wang et al., 2019). Several researchers (Stefanidou & Kappos (2019), Mander & Basöz (1999) and Karim & Yamazaki (2001) have indicated that some seismic fragility studies of bridges utilise single degree of freedom (SDOF) or equivalent static methods to calculate bridge fragility; however, these researchers also agree upon the conclusion that bridge fragility is largely influenced by the condition of the foundation soil. These researchers have noted that the use of oversimplified modification factors for site conditions, as is often done in older methods, is often inadequate.

i) The median increase (approximate) in drift and base shear for fixed-base vs flexible-base (with pile-group SSI) bridges during near-fault motions was 27% in drift and 30% in base shear; the demand for drift increased by as much as 77%, and base shear decreased by 51% due to SSI, thereby significantly altering the fragility (Khurshid et al., 2025).

ii) Fragility results for skewed bridges become more sensitive to the directional and method of estimating demand for ground motion, as a result of SSI impacts; compared to models without SSI, the fixed-base model had greater sensitivity to both these factors (Noori et al., 2019b).

iii) High probabilities of exceedance were produced at low ground motion intensities and columns controlled fragility of the system for fixed-base (no GSI) bridges; therefore, the use of compliant soil systems decreased the vulnerability of bridges with geotechnical seismic isolation (Forcellini & Alzabeebee, 2023).

2.5 THESIS METHODOLOGY

The Performance-Based Earthquake Engineering (PBEE) method has been selected as a framework for this study to achieve the research objectives presented in Section 1.2. The framework will integrate a suite of N bidirectional Synthetic Volcanic Ground Motions with advanced numerical modelling to obtain the fragility curves of both component-level and global fragility functions, where *j* refers to each component and k to each damage state. A summary of the general workflow of the research is provided in Figure 2-10.

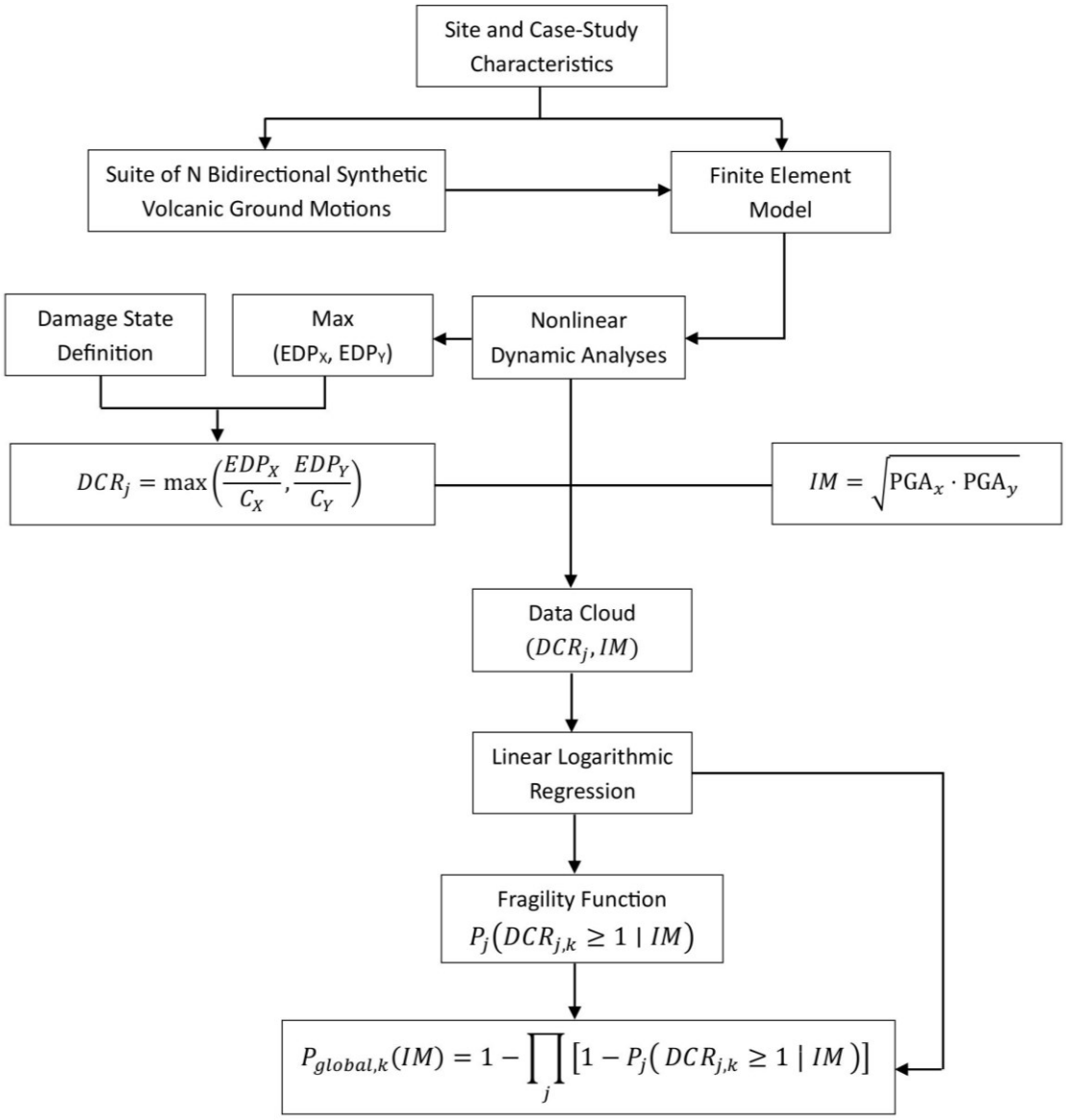

Figure 2-10 Flow chart of the study methodology

3 CASE STUDIES-DESCRIPTION

3.1 BRIDGE DESCRIPTION AND GEOMETRIC CONFIGURATION

My case concerns a highway bridge along the Tangenziale di Napoli (A56) in the municipality of Pozzuoli (Naples), which crosses Via Fascione. Constructed around the early 1970s, the bridge serves as a critical infrastructure link within the Phlegraean Fields (Campi Flegrei) area. SEE Figure 3-2.

The superstructure of the bridge comprises two simply supported spans, a reinforced concrete (RCC) structure 17 m long, utilising precast I-girders placed at a spacing of 1.3 m from each other. The superstructure is supported on thin unreinforced elastomeric pad bearings. The pier features a rectangular section connected at the top by an inverted T-cap beam with double cantilevers, which transfer the deck loads to the vertical piers with an average clear height of 6.5 m.

Figure 3-1 Case study bridge P673 on the Tangenziale di Napoli (A56) crossing over Via Fascione

In this study, three representative cases are developed for the same bridge configuration, differing in bearing type and orientations of the axes, as shown in Table 3-1, and generic elevation and plan configurations and associated details as shown in Figure 3-2.

Table 3-1 Three representative cases of bridge configurations

Case		**Case-1**	**Case-2**	**Case-3**
Bearing type		(Fixed/Roller)	Friction-Type Bearings (Thin unreinforced elastomeric pad bearings)	
Boundary Conditions	**Pier**	Fully fixed in translations, free rotations	Bearings with high vertical stiffness and finite horizontal stiffness, free rotations	
	Abut.	Roller: Free (Long.), Fixed (Trans.), Free rotation.		
Axes Orientation		Orthogonal (0°)		Skewed (30°)

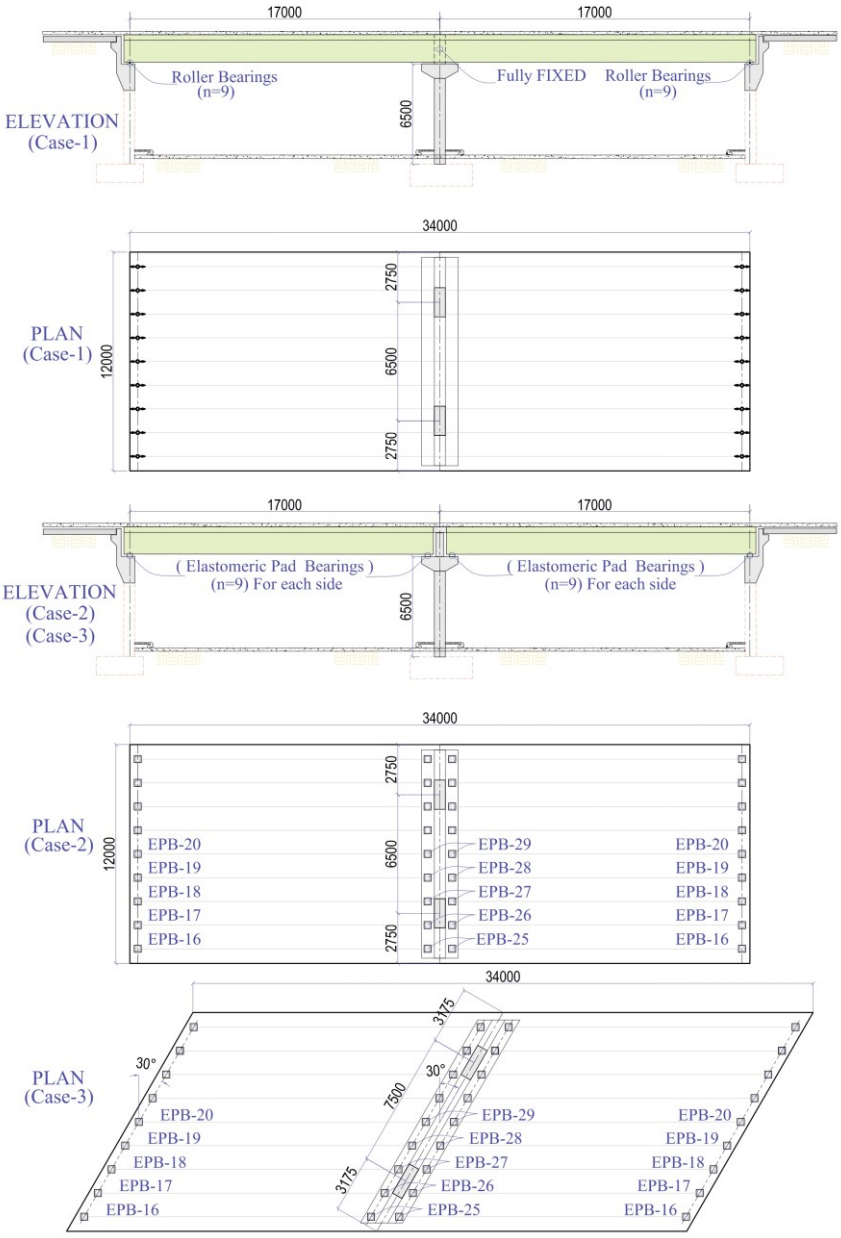

Figure 3-2 Generic elevation and plan configurations

3.2 SEISMIC CHARACTERISTICS AND SEISMIC INPUT

Naples is affected by four sources of shaking: large Apennine tectonic earthquakes, and smaller but closer volcano-tectonic earthquakes from Ischia Island, Campi Flegrei and Vesuvius, SEE Figure 3-3, where the earthquakes are characterised by shallow local depths and low to moderate magnitudes. Despite their relatively small magnitudes, Vesuvian volcanic earthquakes, with hypocenters at approximately 6 km depth, generate intensities one to two degrees higher than tectonic earthquakes of similar magnitude in the nearby Apennine chain (Nappi et al., 2021; Nunziata & Vaccari-a; Rolandi et al., 2025; Scandone et al., 1993).

Figure 3-3 Location of the bridge relative to volcanic sources

Although Naples is not located within a seismogenic zone, it is regularly affected by earthquakes originating in the Southern Apennines, such as the 1980 Irpinia earthquake, which occurred approximately 90 kilometres away. Historical records indicate that damage in Naples is often severe due to local soil conditions and structural deterioration, despite the highest expected intensity being VII–VIII on the MCS scale. The interaction of geographic location, seismic classification, and soil conditions increases this heightened vulnerability (Nunziata & Vaccari-b).

On October 9, 1999, an event was recorded by an instrumental seismic record (MD = 3.6). For a large, destructive historical earthquake such as the A.D. 62 event ($M \approx 5.1 \pm 0.3$), there are no instrumental recordings, and knowledge is derived from macroseismic observations and archaeological evidence. Artificial records generated to be calibrated against macroseismic fields, felt index distributions, and validated ground-motion simulations provide a robust means to reconstruct realistic shaking scenarios (Cubellis & Marturano, 2013). This validation indicates that artificially generated volcanic records can reliably capture the source

characteristics, attenuation behaviour, and intensity distribution typical of Vesuvian earthquakes. Figure 3-4 presents 90 artificial records are used in this study. This is Consistent with previous researchers who developed Fragility curves for highway bridges in the Central and Southeastern United States using 96 synthetic ground motions and full nonlinear time-history analyses (NLTHA) on various bridge models (Nielson & DesRoches, 2007b).

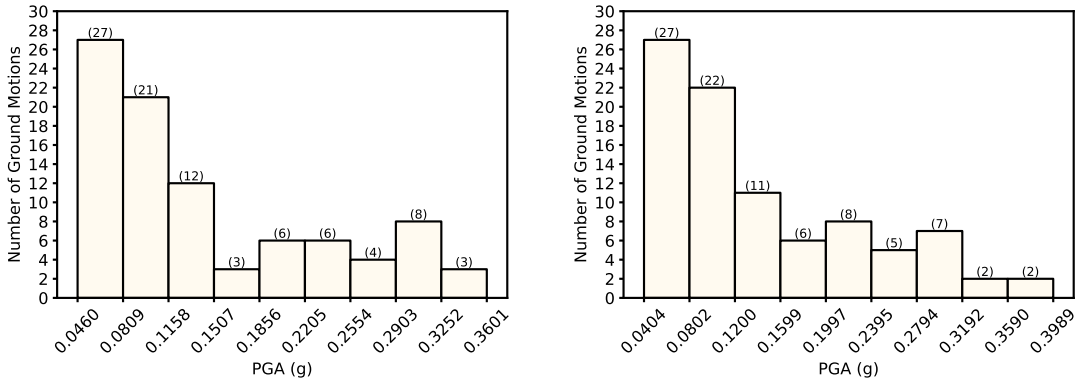

(a) (b)

Figure 3-4 Distribution of PGA for (a) Direction_1, and (b) Direction_2

Volcanic events are frequently modelled as many overlapping low-frequency volcanic earthquakes, not discrete high-frequency shocks (Barajas et al., 2023). Low-frequency volcanic events have longer durations (seconds to minutes) than comparable tectonic quakes of the same magnitude (Lapins et al., 2020; Shuler et al., 2013). As illustrated for one of our categories in Figure 3-5.

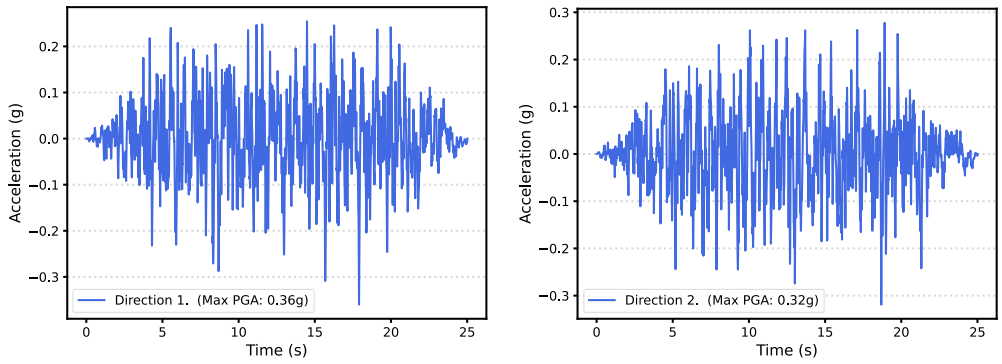

(a) (b)

Figure 3-5 Acceleration History for category 9-10 (a) Direction_1, and (b) Direction_2

4 MODELING AND FRAGILITY DEVELOPMENT

4.1 NUMERICAL MODELLING

The finite element method is employed to analyse three FE models for the same bridge with different configurations. The three models are analysed using scripts written in the Tcl programming language using OpenSees V3.8.0, developed by the Pacific Earthquake Engineering Research Centre at the University of California, Berkeley, and validated by MIDAS CIVIL. Figure 4-1 Shows the three Midas models; In case 1, the pier connection is idealised with low stiffness in all rotational degrees of freedom and extremely high stiffness in all translational degrees of freedom, which permits free rotations. The connection at the abutment is modelled as a roller support, defined by low stiffness in all rotational degrees of freedom and in longitudinal, and high stiffness in vertical and transverse translation. Unlike that in the previous case, the connection between the substructure and superstructure in cases 2 and 3 incorporates thin unreinforced elastomeric pad bearings at both the pier and abutment. Case-2 represents the orthogonal (0°) configuration, while Case-3 introduces a 30° skew.

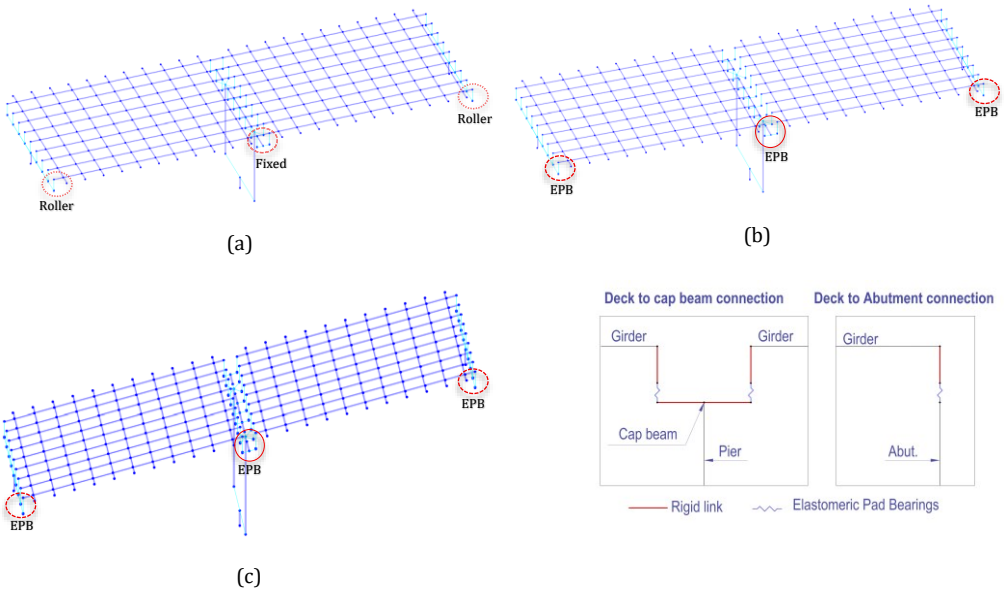

Figure 4-1 3D finite element model of the three configurations;(a) case-1: fixed pier connection case, (b) case-2: friction orthogonal case, and (c) case-3: skewed friction case

4.1.1 Material Modelling

The bridge deck and the abutment material were assumed to behave as elastic elements. The deck was assigned elastic properties, a Young's modulus $E_c = 3.0 \times 10^7 kN/m2$ and a shear modulus $G_c = 1.25 \times 10^7\ kN/m2$. Similarly, the abutments were modelled using elastic material properties with very high stiffness values, a Young's modulus of $E_c = 1.0 \times 10^8 kN/m2$ and a shear modulus of $G_c = 4.17 \times 10^7\ kN/m2$.

The steel material is modelled as an inelastic material using the uniaxialMaterial Steel01, which represents bilinear elastoplastic stress–strain behaviour. The model is defined by the yield strength, initial elastic modulus, and post-yield strain-hardening ratio, allowing accurate simulation of cyclic hysteretic response with kinematic hardening under cyclic loading, as shown in (a) Figure 4-2. Concrete is modelled as an inelastic material using the uniaxialMaterial Concrete01 (Kent–Scott–Park) material model with no tensile strength. The model is defined by the concrete compressive strength, corresponding peak strain, crushing strength, and ultimate crushing strain, enabling realistic simulation of concrete behaviour under cyclic compression, as shown in (b) Figure 4-2.

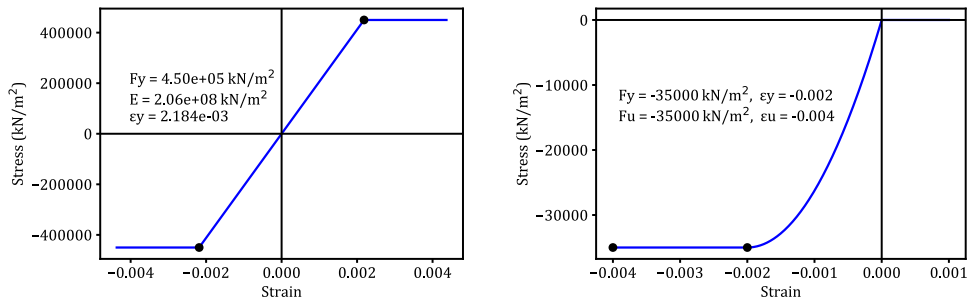

(a) (b)

Figure 4-2 (a) uniaxial material steel01, and (b)uniaxial material concrete01

4.1.2 Sections Properties

To focus on the local structural response of bridge components, particularly the cap beam and bearings, the single-spine beam idealisation is not adopted. Instead, a grillage modelling approach is employed to more accurately capture load distribution and localised effects within the substructure elements, and based on the geometric characteristics of my case, the length-to-width ratio is equal to $\frac{17}{12} = 1.417$ (American Association of State Highway and Transportation Officials, 2020).

"If the span length of a superstructure with torsionally stiff closed cross-sections exceeds 2.5 times its width, the superstructure may be idealised as a single-spine beam. The following dimensional definitions shall be used to apply this criterion:

- Width—the core width of a monolithic deck or the average distance between the outside faces of exterior web.
- Length for rectangular simply supported bridges—the distance between deck joints. Length for continuous and/or skewed bridges—the length of the longest side of the rectangle that can be drawn within the plan view of the width of the smallest span, as defined herein.
- The length-to-width restriction specified above does not apply to concrete box girder bridges".

The determination of a suitable grillage mesh for a beam-and-slab deck, incorporating both longitudinal and transverse elements, is best achieved by considering the specific structural behaviour of the deck to accurately capture its real response (*Bridge Deck Behaviour-Hambly*). Figure 4-3 illustrates sections represented by longitudinal grillage members.

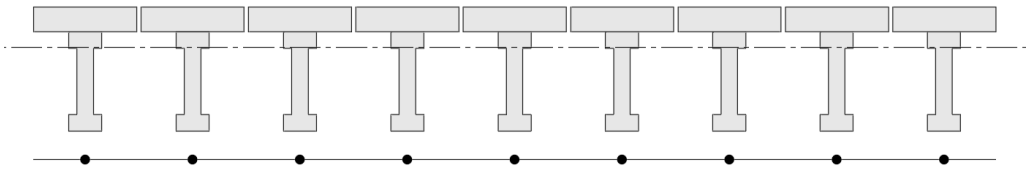

Figure 4-3 Sections represented by longitudinal grillage members

For the grillage members, the flexural moments of flexural are calculated about the centroid of the representative cross section (Bridge Deck Behaviour-Hambly). In non-seismically isolated bridge structures, the cap beam is discretised using fibre-based components and modelled accordingly. It is hypothesised that flexural behaviour governs the critical damage mechanism [Wei, B.; Wang, W.; Wang, T.; Jiang, L.; Wang, T.]. Figure 4-4 shows that the cap beam is represented as an inverted reinforced concrete T-section, while the column is modelled as a rectangular reinforced concrete section. Both sections are discretised into two constituent materials: steel reinforcement and unconfined concrete, using fibre-based elements. The uniaxialMaterial Steel01 is used to represent the reinforcing steel bars, and the uniaxialMaterial Concrete01 material is used to model the concrete fibres for the gross section. The forceBeamColumn element formulation is utilised to implement these fibre sections, using "elementforceBeamColumn $eleTag $iNode $jNode $transfTag "IntegrationType" $maxIters," which employs

Lobatto integration, in addition to incorporating the P-Delta effects to accurately capture the distributed nonlinear flexural response along the element length.

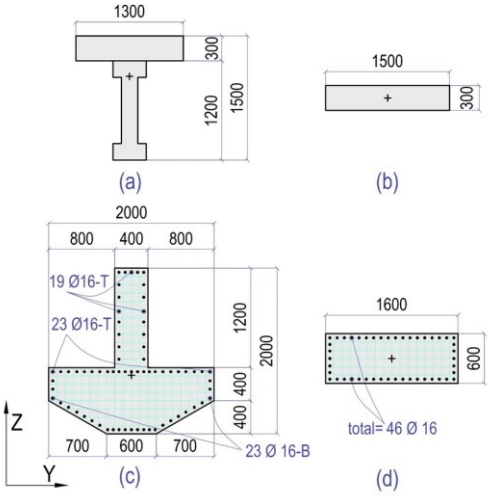

Longitudinal & Transverse Element Properties

Property	Symbol	Value-long element (a)	Value-Trans. Element (b)	Units
Cross-sectional area	A_long	0.7100	0.4500	m²
Torsional constant	J_long	4.37E-02	1.18E-02	m4
Area inertia (y-axis)	I_y,long	1.51E-01	3.38E-03	m4
Area inertia (z-axis)	I_z,long	5.76E-02	8.44E-02	m4

Cap Beam & Column Properties (Fiber Sections)

Property	Symbol	Value-Cap Beam (c)	Value-COLUMN (d)	Units
Cross-sectional area	A_cap	1.8000	0.9600	m²
Shear stiffness (Y)	K_Vy	1.54E+07	1.00E+07	kN/m
Shear stiffness (Z)	K_Vz	1.00E+07	1.00E+07	kN/m
Torsional stiffness	G·J	2.81E+06	1.10E+06	kN·m²
Total reinforcement area	n·A_b	1.10E-02	7.36E-03	m²
Reinforcement ratio(ρ)	As / Ac	0.613	0.76	%

Figure 4-4 (a) Longitudinal Grillage sections (b) Transverse Grillage sections (c) Cap Beam (Fibre Section) (d) Column (Fibre Section)

The abutment is modelled as an elastic element with high stiffness in both longitudinal and transverse directions. It is treated as a rigid support with the properties specified in Table 4-1, while enabling realistic force transfer to the deck and bearing.

Table 4-1 Abutment Element Properties

Property	Symbol	Value	Units
Cross-sectional area	$A_{\text{abut.}}$	100	m^2
Torsional constant	J	1,408.3	$KN{\cdot}m^2$
Second moment of area (y-axis)	I_y	833.33	$KN{\cdot}m^2$
Second moment of area (z-axis)	I_z	833.33	$KN{\cdot}m^2$

Historically, most seismic fragility curves for bridges have been developed specifically for those supported on fixed-base foundations; therefore, the analysis assumed the foundation to be fully fixed. For rocking shallow foundations, accounting for foundation flexibility and soil yielding is essential to control vulnerability; however, assuming a fixed base may be unconservative (Deviprasad et al., 2022).

4.1.3 Mechanical Properties of the Bearings

These bearings, commonly used in bridges built during the 1960s and 1970s, are highly vulnerable to seismic loading. (Minnucci et al., 2022) confirmed that these bearings are "extremely vulnerable components" whose failure increases the overall collapse fragility of the bridge. The bridge bearings are modelled using nonlinear elastic bilinear links via the element twoNodeLink in OpenSees, which captures hysteretic response without isotropic hardening. The bearing reaction is indicated by the yield force, which is defined as $Fy_{Y-Z} = \min(F_{friction}, F_{rupture})$. *T*o determine the mechanical properties of the bearings, the dimensions are estimated due to the absence of specific geometric data, using the median of possible values in literature for the average vertical stress on the bearing ≈ 3 MPa (Ozsarac et al., 2023). Based on the vertical reaction $F_z = 186$ KN from the numerical model, the bearing area is calculated as:

$$A = \frac{F_z}{\sigma_{median}} = \frac{186}{3000} = 0.062\ m^2 \approx 0.25\ m \text{ For each side.} \quad (4\text{-}1)$$

The shear forces in the two horizontal translational degrees of freedom, Fx and Fy, are governed by a circular yield surface. The diameter of this circle, representing the maximum force capacity and computed at each analysis time step, is determined by the lesser value between the friction mechanism and the shear failure of the neoprene pads (shear rupture) (Minnucci et al; Ozsarac et al), SEE Figure 4-5.

$$F_{max} = \min(F_{friction}, F_{rupture})$$

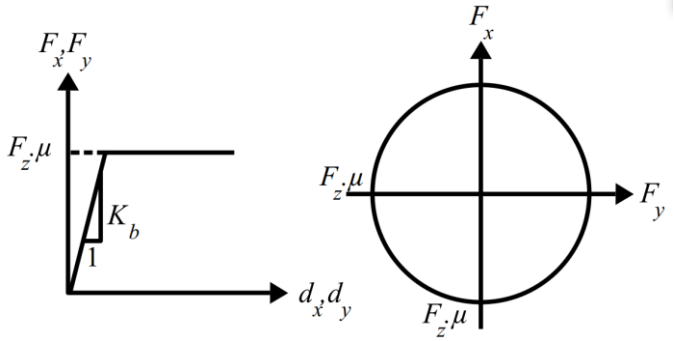

(a) (b)

Figure 4-5 (a) Monotonic shear-deformation relationship (b) Circular yield-surface in shear for the

Friction Limit ($F_{friction}$): This indicates the force at which the bearing starts to slide against the concrete surface.

$$F_{friction} = \mu_0 \cdot Fz = 0.25 * 186 = 46.5\ KN \quad (4\text{-}2)$$

Where: μ_0: Friction coefficient between concrete and neoprene pad bearing range (0.1 to 0.5), and assumed= 0.25 (Minnucci et al.; Ozsarac et al.), and Fz: Vertical load on the pad bearings from the 3D finite element model = 186 KN.

The elastic stiffness for modelling purposes in both directions is given as follows:

$$K_b = \frac{F_{friction}}{d_y} = \frac{46.5}{0.04} = 1162.5\ \text{KN/m} \quad (4\text{-}3)$$

Where: d_y yield displacement assumed $d_y = 0.8 * 0.05 = 0.04m$. Neoprene bearing pads in bridges mainly fail in shear when deformation limits are exceeded. Repeated experimental tests revealed significant damage when shear deformations reached approximately ≈ 50–95% of the pad thickness (Brielmaier & Hoblitzell.; Iqbal & Head, 2024; Ozell & Diniz.).

Shear Rupture Limit ($F_{rupture}$): This indicates the force needed to physically tear the neoprene material.

$$F_{rupture} = \gamma_{lim} \cdot G \cdot A = 1 * 1000 * 0.625 = 62.5\ KN \quad (4\text{-}4)$$

γ_{lim}: Maximum allowable shear strain (assumed to be 1.0), according to Minnucci et al, and G: The shear Modulus is adopted $G = 1000\ \text{kN/m}^2$ within the range (0.90–1.38 MPa) of semi-rigid specified by (AASHTO, 2020). Neoprene bearing supports, classified as having semi-rigid mechanical behaviour, are characteristic of Italian bridges designed in the 1970s (Gauron et al., 2018; Minnucci et al., 2022).

The elastic stiffness for modelling purposes in both directions is expressed as:

$$K_b = \frac{G_r A_r}{t_r} = \frac{1000 * 0.0625}{0.05} = 1250\ \text{KN/m} \quad (4\text{-}5)$$

Where: G_r is the rubber shear modulus, A_r is the bearing area in plan, t_r is the total rubber thickness.

The models considered the lower horizontal elastic stiffness in both directions, as calculated from Equation (4-3) and Equation (4-5).

4.1.4 Damping Model

Accurately modelling energy dissipation mechanisms presents significant challenges in the dynamic analysis of structures, particularly in nonlinear response history analysis (NRHA), due to the various sources of damping, including material hysteresis, friction, and interactions between structural and nonstructural components. There are two main perspectives on incorporating damping in structural analysis:

- (Priestley & Grant, 2005) proposed that a more realistic assumption for inelastic systems is to employ simply the tangent-stiffness proportional damping. Additionally, (Petrini et al., 2008) Compared computational and experimental data for a bridge pier that experienced significant inelasticity to validate this modelling approach.
- (Chopra & McKenna, 2016) clarified that this method does not have a physical basis since, for large displacements, the negative stiffness leads to negative damping values. As an alternative, they proposed constant modal damping.

In the current study, two predominant vibration modes of the numerical model were utilised to calibrate the damping coefficients for traditional mass- and stiffness-proportional Rayleigh damping, as typically reported in (Chopra, A.K. - Dynamics of Structures - Theory and Applications to Earthquake Engineering (4th Ed)) , with a target damping of 2% during seismic stimulation. The coefficients a_0 and a_1 in the formula are computed based on the periods T_1 and T_2, as illustrated in the Figure 4-6.

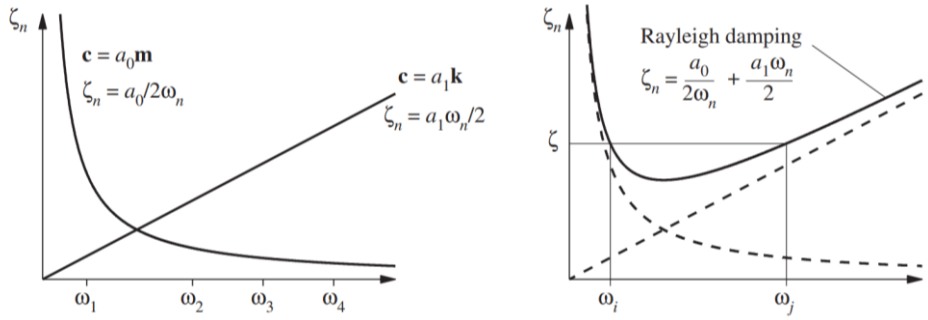

(a) (b)

Figure 4-6 Changing in modal damping ratios with natural frequency: (a) mass-proportional and stiffness-proportional damping; (b) Rayleigh damping

In Rayleigh damping, the mass matrix M and the stiffness matrix K are assumed to be linearly combined to form the viscous damping matrix C, as expressed in Rayleigh damping as:

$$C = a_0 M + a_1 K \tag{4-6}$$

where a_0 and a_1 are the mass-proportional and stiffness-proportional damping coefficients, respectively. Using undamped mode shapes keeps the damping matrix diagonalizable, maintaining modal uncoupling in linear dynamic analysis. Rayleigh damping defines the damping ratio for the -th mode as follows:

$$\zeta_n = \frac{a_0}{2\omega_n} + \frac{a_1 \omega_n}{2} \tag{4-7}$$

where ω_n denotes the natural circular frequency. This statement shows how the damping ratio varies with frequency, with the stiffness-proportional term dominating at high frequencies and the mass-proportional term at low frequencies. Rayleigh damping doesn't produce a constant damping ratio across all modes but approximates experimental damping over a limited frequency range. The Rayleigh coefficients are calculated as follows, considering equal damping ratios. ζ for the i-th and j-th modes:

$$a_0 = \zeta \frac{2\omega_i \omega_j}{\omega_i + \omega_j}, \qquad a_1 = \zeta \frac{2}{\omega_i + \omega_j} \tag{4-8}$$

After the coefficients are determined, the damping matrix is explicitly defined and applied consistently throughout the dynamic analysis. Table 4-2 shows the calibrated damping coefficient parameters for each configuration (a_0 and a_1). The values were calculated using the first two natural time periods (T_1 and T_2) to achieve the target damping ratio of 2%. The difference in coefficient values is due to the influence of structural configuration and the boundary conditions.

Table 4-2 Rayeleh Damping coefficients

Case	Case-1	Case-2	Case-3
T1 (s)	0.6423	0.9742	0.9824
T2 (s)	0.1035	0.8561	0.8564
Damping	2.0 %	2.0 %	2.0 %
$\boldsymbol{a_0}$	0.336990362	0.137314873	0.13668012
$\boldsymbol{a_1}$	0.000567461	0.002900885	0.00291280

4.2 DEVELOPMENT OF FRAGILITY CURVES

The analytical methodology for generating fragility curves in this study is based on comprehensive, nonlinear, dynamic time-history analyses that quantify seismic demands on bridge components. Seismic demand is characterised by displacement for the elastomeric pad bearings and curvature for structural sections (pier and cap beam). The fundamental fragility formulation quantifies the probability that, for a given Peak Ground Acceleration (PGA), the demand on a bridge component equals or exceeds a specific damage state limit, corresponding to a defined performance limit state as described in the following section 4.2.1. This approach assumes that both seismic demand and structural capacity are lognormally distributed (Nielson & DesRoches, 2007b). The bridge component fragility can be expressed as:

$$P_j\left(DCR_{j,k} \geq 1 \mid IM\right) = \Phi\left[\frac{ln\left(\frac{S_d}{S_c}\right)}{\sqrt{\beta_{d|IM}^2 + \beta_c^2}}\right] = \Phi\left(\frac{ln(IM) - ln(\theta)}{\beta_{DCR\backslash IM,k}}\right) \qquad (4\text{-}9)$$

Where: $\Phi(\cdot)$ is the standard normal cumulative distribution function (CDF); β is the total dispersion with respect to the IM, the parameter combines demand uncertainty, quantified by the logarithmic standard deviation of the demand ($\beta_{d|IM}$) and capacity uncertainty (β_c); θ is the median capacity in terms of IM, for which there is a 50% probability of exceeding the damage state.

Finally, the global system fragility curves, $P(F_{system})$, were determined numerically as the upper bound in Equation expressed as:

$$P_{global,k}(IM) = 1 - \prod_j \left[1 - P_j\left(DCR_{j,k} \geq 1 \mid IM\right)\right] \qquad 4\text{-}10)$$

The result of the global fragility curve represents the probability that at least one critical component reaches or exceeds damage state k.

4.2.1 Damage State Limits

Reasurches have shown that section curvature, material strain, and bearing deformations can be used to determine the damage stage of structures and components. In addition to the characterisation of damage to global bridges resulting from direct physical damage described in section 2.3.6, it will also be necessary to define component damage states using physically based threshold

values; thus, a moment-curvature analysis was conducted using SAP2000. V.26.0.0 software to quantify the damage state limits at each critical cross-section according to (Priestley & Kowalsky, 1998; Zhou et al., 2024). Moment-curvature curve limits for longitudinal or transverse direction, and damage characteristics are provided in Table 4-3.

Table 4-3 Damage characteristics and criteria for various damage states

Damage State	Damage Characteristics	Limiting Strain Criteria (whichever occurs first)
None (DLS-0)	No steel yield, only tiny cracks	$\phi < \phi'_y$ (initial)
Slight (DLS-1)	First Yield: First yielding of longitudinal bars, Surface concrete cracks, and even spalling.	$\phi = \phi'_y$ (initial) $\epsilon_s = \frac{f_y}{E_s}$ (Yield strain steel) $\epsilon_c = 0.002$
Moderate (DLS-2)	Nonlinear deformation occurs locally, and a plastic hinge appears.	The bilinear of yield: $\phi_y = \phi'_y \times (M_n/M_y)$
Extensive (DLS-3)	Plastic hinge is fully formed, a large crack appears, and the surface concrete of the whole plastic hinge is spalling.	$\epsilon_s = 0.015$ $\epsilon_c = 0.004$
Complete (DLS-4)	Strength degrades, Longitudinal bars yield, and core concrete crushing	$\epsilon_s = 0.060$ $\epsilon_c = 0.018$

The limit of minor damage is indicated by the curvature of the longitudinal rebar at the first yield (φ1), the limit of moderate damage by the equivalent yield curvature (φy), the limit of severe damage by the curvature associated with concrete spalling in the protective layer (φb), and the ultimate yield curvature (φu) (Zhou et al., 2024), as shown in Figure 4-7.

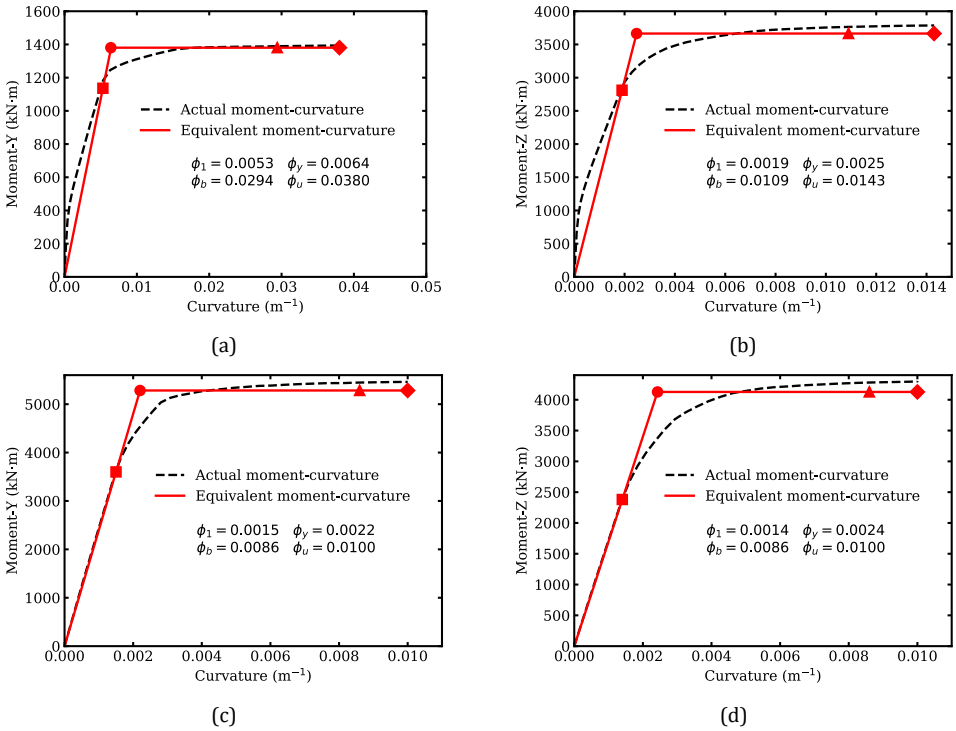

Figure 4-7 Bending moment–curvature diagrams of key sections for pier columns and cap beam. (a) pier bottom section around weak axis (b) pier bottom section around strong axis (c) cap beam section around strong axis y-y (d) cap-beam section around weak axis z-z

Similarly, the limits of bearing damage on the bridge were described in four discrete Damage Limit States (DLSs), determined by the relative displacement capacity of bearings, which corresponds to the bearings and concrete surfaces. The thresholds for slight and moderate damage (DLS-1 and DLS-2) are followed (Nielson & DesRoches, 2007c; Ozsarac et al., 2023). Conversely, the extensive and complete damage states (DLS-3 and DLS-4) are governed by the physical geometry of the cap beams, which determine that DLS-3 corresponds to the situation where the bearing is dislocated from the supporting concrete pedestal. Lastly, DLS-4 refers to the situation where the bridge deck falls from the cap beam due to the sliding of bearings (Borzi et al., 2015c). SEE Table 4-4.

Table 4-4 Definition of Damage Limit States for Bearings

Damage State	Damage Description	Relative displacement
DLS-1 (Slight)	corresponds to the initiation of bearing yielding	40 mm
DLS-2 (Moderate)	Excessive sliding occurs, and and the bridge deck will likely need to be aligned to become fully operational again	100 mm
DLS-3 (Extensive)	Dislocation of the bearing from the supporting concrete pedestal	300 mm
DLS-4 (Complete)	Unseating of the bridge deck from the cap beam, leading to the deck fall	550 mm

4.2.2 Probabilistic Seismic Demand

The methodology of analytical fragility functions is based on the Cloud Analysis method within the probabilistic performance-based earthquake engineering (PBEE) framework (Cornell et al., 2002). Cloud Analysis requires fewer analyses than Multiple Stripe Analysis (MSA) while maintaining the same level of IDA fidelity, making it ideal for component-level assessment (Baker, 2015). The parameters S_d and $\beta_{d|IM,k}$ are estimated using Cornell's methodology. In which the median seismic demand is assumed to follow a power-law function with respect to the selected intensity measure (IM). This relationship is expressed as:

$$S_d = DCR_k = a_k.(IM)^{b_k} \tag{4-11}$$

where a_k and b_k regression coefficients for each damage state k, represent the intercept and the slope, respectively. These parameters are determined through the following procedure:

1. Perform a Monte Carlo simulation where a suite of N Ground motions are paired with 3D analytical bridge models, and nonlinear time-history analyses are conducted for each ground motion-structure combination.
2. Record the peak seismic Demand-to-Capacity Ratio (DCR) corresponding to each (PGA_{geo}).
3. Perform a regression analysis on the $\ln(DCR)$ vs $\ln(PGA\_geo)$ data pairs.

The geometric mean was selected for the intensity measurement because the geometric mean is a better method of reducing the variance of data for each individual record when compared to the horizontal component alone. This will increase the regression stability and accuracy of the hazard calculations. In

addition, (Pinzón et al., 2024) reported that, based on an analysis of some previous research studies completed in Italy and Costa Rica, there was very little difference (~1-3%) between the orientation-independent GMRotD50 values and those measured directly using a geometric mean. These results confirm that there are a low level of bias and a high level of stability in this type of analysis.

$$IM = \mathrm{PGA}_{geo} = \sqrt{PGA_x \cdot PGA_y} \tag{4-12}$$

The seismic performance of bridge types is measured using a systemically decoupled bidirectional demand–capacity ratio of the form shown below. This approach works well when one direction clearly dominates the response, and ensures safety is controlled by the most critical direction, analogous to using the highest $\frac{\mathrm{D}}{\mathrm{C}}$ among multiple failure modes (X-Y directions) (Jalayer et al., 2016).

$$DCR_{j,k} = \max\left(\frac{D_{j,L}}{C_{j,L}^{(k)}}, \frac{D_{j,T}}{C_{j,T}^{(k)}}\right) \tag{4-13}$$

where: $D_{j,L}$ and $D_{j,T}$ the max absolute longitudinal and transverse demand, respectively, $C_{j,L}^{(k)}$ and $C_{j,T}^{(k)}$ represent the capacities for damage state k.

The bridge system is modelled as a series of components, which means that if a critical component exceeds its limit state, global damage is considered. Consequently, the global relationship between demand and capacity is defined as:

$$DCR_{global,k} = \max_j\left(DCR_{j,k}\right) \tag{4-14}$$

where j spans all active components in the structural configuration:

- Fixed pier system: pier + cap beam
- Friction systems: pier + bearing + cap beam

The parameter of the median Capacity in terms of IM (θ) is expressed by inverting the power-law demand model:

$$PGA_{geo-50\%} = ln(\,\theta\,) = \frac{ln(DCR) - ln(a)}{b} \tag{4-15}$$

The dispersion of the seismic demand ($\beta_{d|PGA,k}$) is subsequently derived from the regression results using Equation:

$$\beta_{DCR|IM,k} = \sqrt{\frac{1}{N-2}\sum_{i=1}^{N}\left[\ln\left(DCR_{i,k}\right) - \left(\ln(a_k) + b_k\ln(IM_i)\right)\right]^2} \qquad (4\text{-}16)$$

The parameter β representing the total Dispersion in terms of (IM) can be estimated by the regression slope b:

$$\beta = \frac{\sqrt{\beta_c^2 + \beta_d^2}}{b} \qquad (4\text{-}17)$$

When the uncertainty related to structural capacity is assumed to be roughly zero, the total dispersion can be expressed as:

$$\beta_{IM} \approx \frac{\beta_{DCR|IM,k}}{|\,b\,|} \qquad (4\text{-}18)$$

5 RESULTS AND DISCUSSION

5.1 VALIDATION OF THE NUMERICAL MODELS

5.1.1 Comparison of Gravity Results

To ensure the reliability of OpenSees models prior to nonlinear dynamic analyses and fragility assessment, a validation study for these models against a fully independent finite element model was performed using MIDAS. The study primarily compared the fundamental periods of the models to confirm the consistency of global dynamic behaviour, as shown in Table 5-1, as well as the support reaction forces under gravity loads in Table 5-2, and the deformations of the three bridge configurations to verify equilibrium, stiffness representation, and boundary condition modelling. Additional details regarding Case 1 and Case 2 are provided in Appendix A.

Table 5-1 Comparison of Modal Periods Between OpenSees and MIDAS for CASE-3

Mode Number	Mode Shape Characterised	OpenSees	MIDAS	Relative OpenSees Midas Discrepancy
1	Full-bridge longitudinal	0.9824	1.0083	2.57%
2	Full-bridge Transversal	0.8564	0.8528	-0.42%
3	Full-bridge Torsional mode, anti-symmetric Transversal displacement	0.8430	0.8420	-0.12%
4	Full-bridge Torsional mode, anti-symmetric longitudinal displacement	0.8397	0.8395	-0.03%

Table 5-2 Support Reaction Forces Between OpenSees and MIDAS for CASE-3

Location/Reaction	FX (kN)	FY (kN)	FY (kN)	MX (KN.m)	MY (KN.m)	MZ (KN.m)
Abutment-MIDAS	9.877	0.968	1678.050	284.278	153.431	8.086
Abutment-OpenSees	9.324	0.800	1678.050	462.890	257.220	8.893
Pier-MIDAS	0.000	0.000	4185.600	0.000	0.000	16.740
Pier-OpenSees	-0.03	-0.05	4185.600	8.060	-4.652	15.570

5.1.2 Comparison of Nonlinear Response History Analysis Results

This section validates the performance of the three bridge configurations through nonlinear response-history analysis of a representative seismic record. The comparison examines the longitudinal force–displacement response at the pier tops, as illustrated in Figure 5-1. The cross-validation between the two programs is very consistent, with excellent agreement in the longitudinal forced-displacement responses of three cases. Case 1 exhibits the highest stiffness and force capacity because the load transfers directly to the substructure. Friction-based elastomeric pad bearings have lower peak forces and more stable hysteretic behaviour due to the energy dissipation at the bearing level. Bearings reduce the transmission force through deformation, as clarified further in the fragility results.

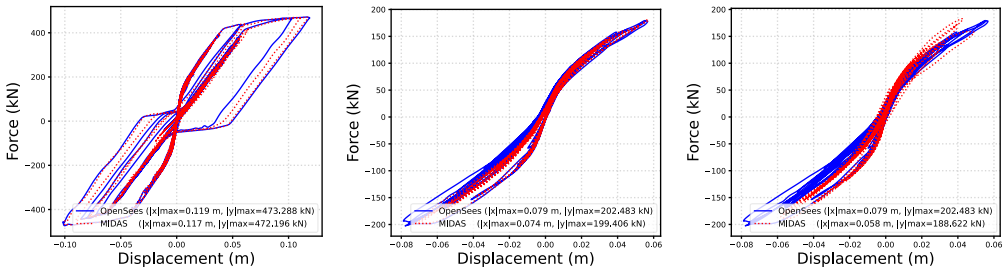

(a) (b) (c)

Figure 5-1 Longitudinl Force-Displacment at top piers for (a) case 1, (b) case 2, (c) case 3

Additional details regarding the moment–curvature relationships for the piers and cap beams, along with the longitudinal and transverse critical bearing force–displacement to confirm the consistency of inelastic behaviour, stiffness degradation, and hysteretic characteristics across the cases analysed, are provided in Appendix B.

To determine the critical elastomeric pad bearing over the pier in the friction cases, a scatter maximum in either the longitudinal or transverse displacements of the bearings is identified, which informs the control bearing-level fragility assessment. Figure 5-2 shows that all bearings aligned along the same axis perform identically, with the notable exception of a slightly higher value for EPB-29.

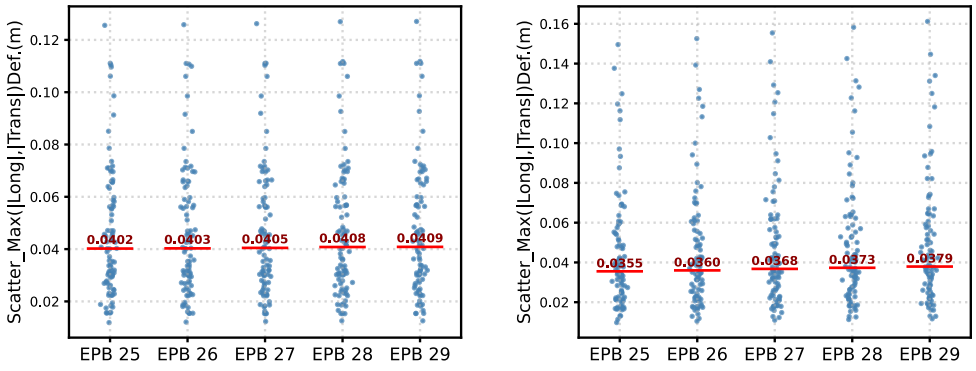

Figure 5-2 Comparison of maximum absolute displacement in either the longitudinal or transverse directions, (a) case-2, and (b) case-3

5.2 FRAGILITY CURVES

5.2.1 Component Fragility Curves

In this section, component bridge fragility curves under artificial bidirectional volcanic earthquakes were developed to quantify how likely each part of a bridge (piers, bearings, cap beams) is to reach specified damage states as ground-motion intensity increases. Subsequently, these component fragilities were integrated into a realistic system-level bridge fragility.

5.2.1.1 Piers

As a first step in developing fragility curves through probabilistic seismic cloud analysis, regression-based demands on the DCR-PGA_{geo} relationships increase with seismic intensity across all damage states. The fixed pier configuration has a higher DCR and demand level because it has higher pier stiffness, making it more vulnerable. Unlike the friction configurations (orthogonal and skewed) axes, which have a lower demand due to the bearing effects, as shown in the Figure 5-3. For additional details about regression analysis for the remaining components (bearings and capbeams), as well as for the global bridge system, are provided in Appendix C.

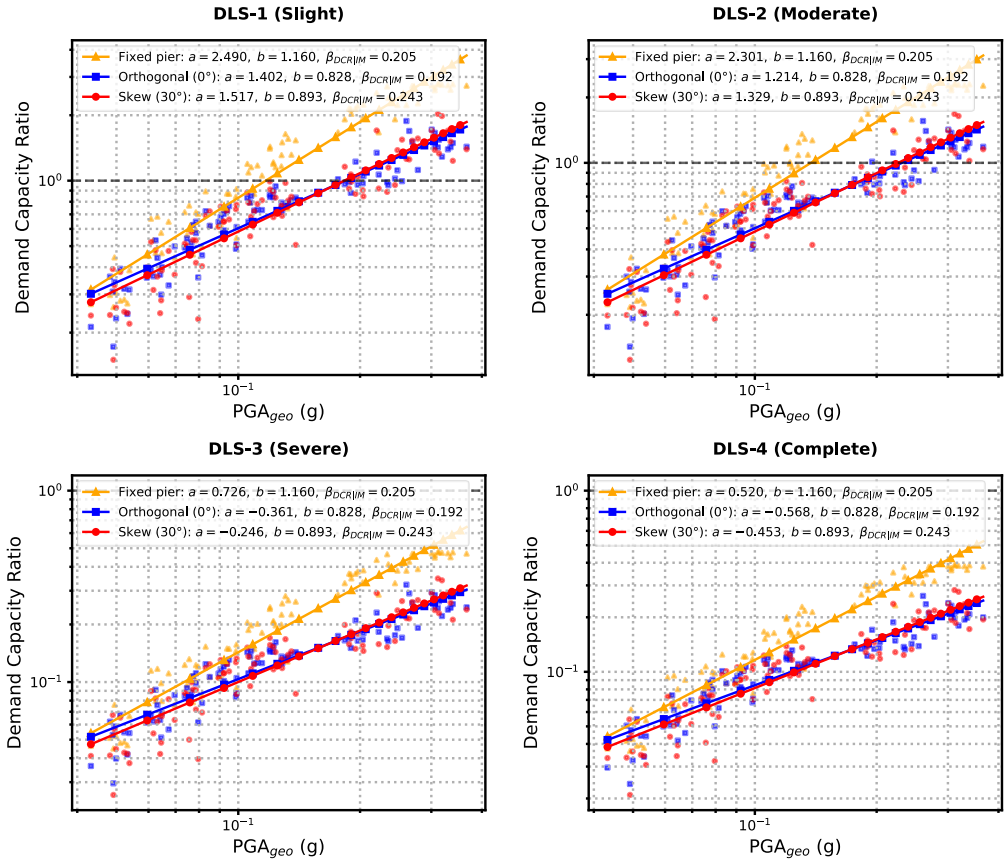

Figure 5-3 Regression-based probabilistic seismic analysis for the piers in the three configurations

The fragility curves results confirm that the fixed configuration reaches higher probabilities of exceedance at lower PGA levels, as shown in Figure 5-4. Elastomeric pad bearings enhance the seismic performance of the bridge by providing isolation between the substructure and the superstructure. The skew configuration produces twisting effects and increases the crack ratio in the structure, thus reducing the capacity, particularly in the severe and complete damage states.

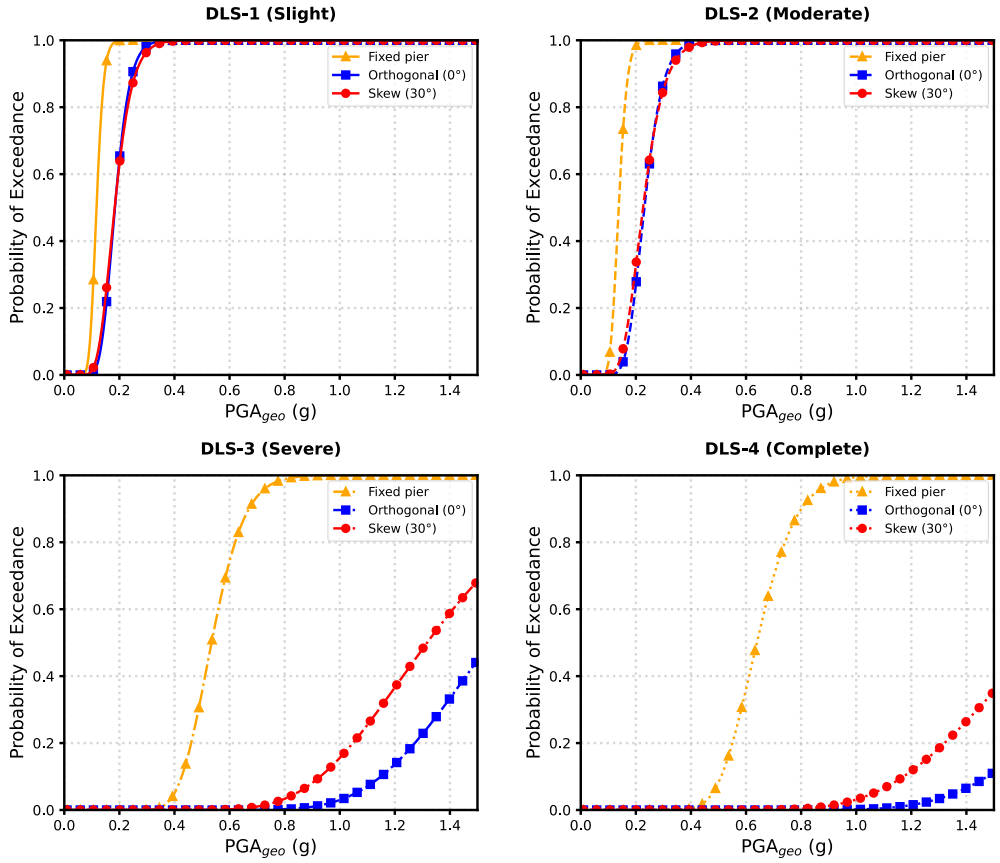

Figure 5-4 Comparison of Fragility Curves for the Piers in three configurations

By examining the differences between the three configurations using the median intensity measure (θ) in Table 5-3 using the below equation.

$$\text{Relative discrepancy} = \frac{\theta_{\text{case 3}} - \theta_{case\ 1,2}}{\theta_{\text{case 1,2}}} * 100 \qquad (5\text{-}1)$$

Comparison of case 3 with case 1 conveys that the bearing increases the pier capacity at all damage levels by ≈ 56–64% for slight damage and moderate damage levels, and by ≈146–160%for severe and complete damage states, respectively. This confirms that adding bearings dramatically enhances the seismic performance. Rotation (30°) has little effect at low damage levels but causes a significant drop in capacity by ≈ 14–16% at high damage levels.

Table 5-3 Median of all pier damage levels for the three cases

Damage State	Case 1 (θ)	Case 2 (θ)	Case 3 (θ)	Relative discrepancy case 1,3	Relative discrepancy case 2,3
Slight	0.1169g	0.1838g	0.1828g	56.37%	-0.54%
Moderate	0.1376g	0.2308g	0.2258g	64.10%	-2.17%
Severe	0.5346g	1.5465g	1.3171g	146.37%	-14.83%
Complete	0.6389g	1.9856g	1.6605g	159.90%	-16.37%

5.2.1.2 Cap beams and bearings

Although bearings enhance the seismic performance of bridges by reducing the force transferred to the substructures, they are constrained by their deformation limits, making them among the most fragile elements of the bridge system, as shown in (b) Figure 5-5. The axis orientation does not have a significant effect on initial damage development (slight and moderate) because the mechanical performance of the bearings is identical in local directions; however, it has a significant effect on damage progression due to the correlation between the pier. Unlike bearings and piers, the cap beams remain predominantly elastic under realistic seismic intensity levels, even accounting for skewness, as shown in (a) Figure 5-5. These results are consistent with those reported in the literature review.

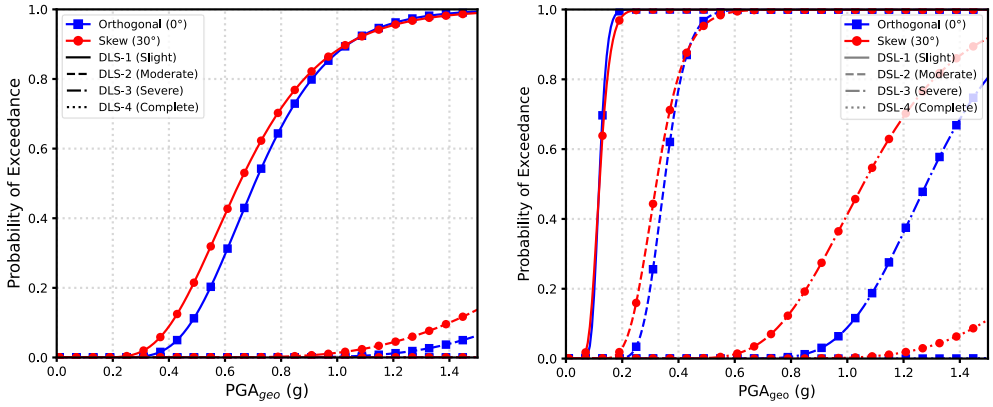

(a) (b)

Figure 5-5 Comparison of component Fragility Curves: (a) for the Cap beam, and (b) for the Critical Bearing over the Piers in the Friction Cases

The relative discrepancy of the median (θ) in Table 5-4 shows differences for the cap beam in the median values of the friction cases (orthogonal and skew), except the fixed-pier configuration from the comparison, as the cap beam in this case exhibts a highly median values, as shown in Appendix D.

For the slight and moderate damage are ≈ 6.5-8.0 %, which can be neglected. The median (θ) values for the cap beam are significantly higher than other components, its median intensity for slight damage is ≈ 4 times that of the pier, while for moderate damage increases to ≈ 10 times in both friction configurations. However, the severity and completeness of damage are significantly higher in both configurations, exceeding realistic seismic intensity levels. This confirms that the cap beam does not act as the key failure component of the bridge system at the investigated hazard levels.

For the critical bearing, the discrepancy between the median of the intensity measure for slight and moderate damage is insignificant ≈ 0.5-8.0%. These results confirm that the initial bearing response is unaffected by axis rotation; however, at severe and complete damage levels, the median (θ) decreases by ≈ 17-22 % for the high damage. These results convey that during strong earthquakes; the skew configuration causes the bearings to be damaged more rapidly.

Table 5-4 Median $PGA_{geo}(g)$ of the critical elastomeric pad bearing for all damage levels

Component	Damage State	Case 2 (θ)	Case 3 (θ)	Relative discrepancy Case 2,3
Cap beam	Slight	0.7057g	0.6508g	-7.78%
	Moderate	2.3806g	2.2255g	-6.52%
	Severe	208.48g	204.91g	-1.71%
	Complete	291.30g	287.37g	-1.35%
Elastomeric pad bearing	Slight	0.1181g	0.1187g	0.51%
	Moderate	0.3491g	0.3208g	-8.11%
	Severe	1.2809g	1.0567g	-17.50%
	Complete	2.6242g	2.0397g	-22.27%

5.2.2 System Fragility Curves

The bridge system is modelled as a series of components, which means that if a critical component exceeds its limit state, global damage is considered. The global fragility parameters developed for each case at each damage state, including Max DCR, median intensity (θ), dispersion (β), and goodness-of-fit (R^2), are summarised in Table 5-5, respectively.

Table 5-5 Global Fragility Parameters for the three cases

Damage State	Cases	Max DCR	θ (Median)	β (Disp)	R^2
(DLS-1) Slight	Case 1	2.783	0.1169g	0.1765	0.921
	Case 2	3.176	0.1177g	0.1796	0.919
	Case 3	4.03	0.116g	0.218	0.885
(DLS-2) Moderate	Case 1	2.304	0.1376g	0.1765	0.921
	Case 2	1.558	0.2318g	0.1900	0.910
	Case 3	1.678	0.2208g	0.1976	0.903
(DLS-3) Severe	Case 1	0.477	0.5346g	0.1765	0.921
	Case 2	0.424	1.3165g	0.1598	0.934
	Case 3	0.537	1.095g	0.1815	0.917
(DLS-4) Complete	Case 1	0.388	0.6389g	0.1765	0.921
	Case 2	0.262	3.3401g	0.1715	0.925
	Case 3	0.293	2.8384g	0.1956	0.905

The comparison of global fragility in Figure 5-6 between fixed-pier and friction configurations shows a significant reduction in overall vulnerability in friction cases at higher damage levels (DLS-3 and DLS-4). Friction systems have shifted the fragility curves to higher PGA values due to energy dissipation and demand redistribution. However, the overall susceptibility to slight damage is the same for all configurations: the fixed pier damage is highly related to the damage of the pier, and bearing systems are affected by the vulnerability of the bearings. For moderate damage levels, it was observed that friction configurations have less overall susceptibility than fixed configurations, due to the energy dissipated by the bearings. The higher fragility in the 30° skew configuration compared to the orthogonal case is mainly due to torsional effects and asymmetric stiffness from geometric irregularity. Additional detailed results, including component-level fragility parameters and regression statistics for each configuration, are presented in Appendix D.

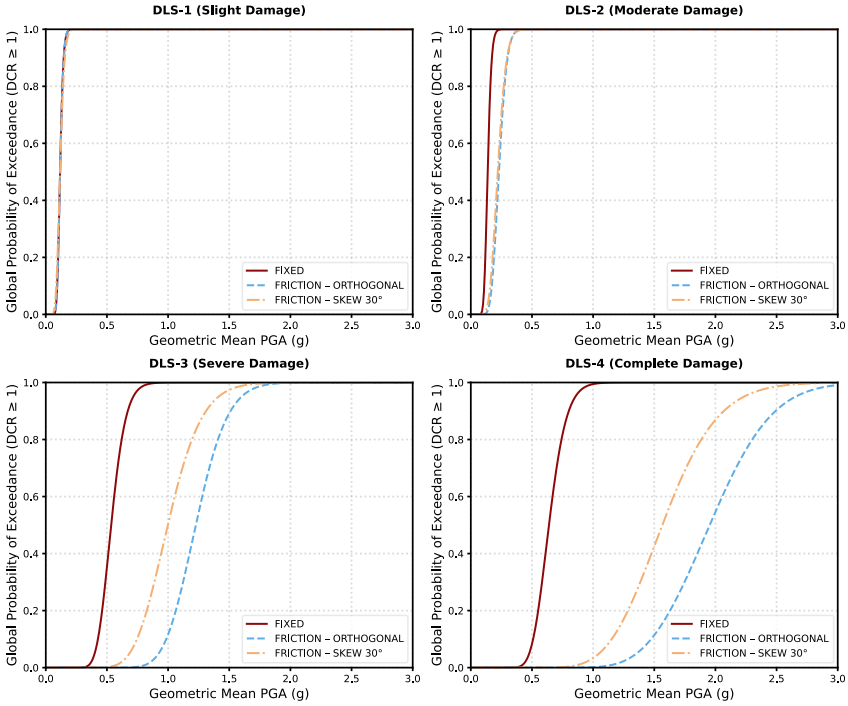

Figure 5-6 Comparison of the global fragility between the three configurations

Comparing the global performance in Table 5-6 across configurations using the median intensity measure (θ), demonstrating that elastomeric pad bearings dramatically enhance seismic performance. While the performance discrepancy is negligible at the slight damage state, the friction-based system increases seismic capacity by ≈ 60.0% for the moderate damage state and by a substantial 86–145% for severe and complete damage states, respectively. While a 30° skew has a minimal impact at initial damage states, it reduces the overall seismic resilience by ≈ 20% at higher damage thresholds.

Table 5-6 Median of global damage levels for the three cases

Damage State	Case 1 (θ)	Case 2 (θ)	Case 3 (θ)	Relative discrepancy case 1,3	Relative discrepancy case 2,3
Slight	0.1169g	0.1177g	0.1168g	-0.07%	-0.50%
Moderate	0.1376g	0.2301g	0.2203g	60.14%	-4.24%
Severe	0.5346g	1.2263g	0.9975g	86.59%	-18.66%
Complete	0.6389g	1.953g	1.5653g	144.99%	-19.85%

6 CONCLUSIONS AND FUTURE WORK

6.1 SUMMARY

This work addressed the seismic vulnerability of a reinforced concrete precast T-girder highway bridge in Naples, Italy, which is located in an area with seismic risks resulting from many volcanic sources. The main objective of this study was to create fragility curves at both the component and system level for this bridge in three configurations with a strong focus on superstructure and substructure interconnectivity, as well as pier rotations, skewness effects with bidirectional volcano-induced ground motion.

To achieve this objective, Dynamic Nonlinear Time History (DNTH) analyses based on a 3D Finite Element Modelling (FEM) framework were developed. The bridge was modelled in three different configurations: with fixed pier connection and idialised roller over the abutment, with a friction for piers and abutments based on a thin unreinforced elastomeric pad bearing, and with a skewed axis of both pier and abutments. To achieve record-to-record variability and combined seismic demand, the same set of ninety synthetic earthquakes from volcanoes was applied to each record in both x and y directions. Curvature-based Engineering Demand Parameters (EDPs) were used on the piers and cap beams to determine damage state limits for the specific components. Based on this, cloud analysis techniques were used to generate probabilistic Fragility Curves for the structure components and global system.

The results demonstrate that the different configurations produced distinct seismic responses and fragility characteristics. For example, demand redistribution among structural components was significantly affected by the implementation of elastomeric pad bearings. Additionally, bidirectional excitation and geometric skewness induce significant torsional effects, which reduces the seismic performance of the bridge. In general, the study provided detailed information about the seismic fragility of girder bridges in Naples. The failure of reinforced concrete girder bridges in the downtown Naples roadway system increases the disaster risk throughout the community by increasing population density and by the ageing of both existing bridges and urban areas. The goal was to provide high-quality data to assist policymakers with finding appropriate funding for retrofitting and preserving both the bridge and the economic stability of the area.

6.2 CONCLUSIONS

This study produced several evidence-based conclusions regarding the seismic performance of existing reinforced concrete girder bridges subjected to bidirectional volcanic ground motions.

First, the interaction between the superstructure and substructure was found to be a major factor in determining seismic fragility. The fixed pier connection with an idealised roller at abutment exhibited very high vulnerability, concentrated mainly in the pier columns, where curvature demands increased drastically with increasing seismic intensity. The addition of a thin unreinforced elastomeric pad bearing changes the transfer of force and decreases the demands on the pier at low to moderate intensity, while adding significant vulnerability to the bearings themselves.

Second, the results indicate that bearings are the most vulnarable component in typical bridge configurations from the 1960-1970 Construction Era under seismic loads. Bearings exhibited significant sliding and shear-related limit states prior to any major damage to the piers, with the amount of damage to the piers being dependent on the maximum ground motion intensity. The damage hierarchy in the friction cases emphasises the dual role of bearings as a fuse that can reduce the load transferred to the substructure. At the same time, it also increases the overall system fragility during earthquake loading. Furthermore, the presence of skewness indicates an insignificant difference in initial damages (slight and moderate) when the bearings' mechanical characteristics are identical in the local directions; however, there is a statistically significant difference in the final damage severity due to the skewness effect. Furthermore, the cap beam consistently exhibited excellent performance for each analysed configuration layout, with damage probability remaining relatively low at any given level of earthquake intensity.

Overall, the results of the present research indicate that the principal goals have been addressed in their entirety. Globally, the fixed case was most vulnerable with significantly smaller intensity measure (θ) compared to the friction configurations. Both friction setups shifted fragility curves to higher intensity levels, indicating better seismic resilience. At upper damage levels, the skew configuration was more vulnarable than the orthogonal case due to torsional demand and asymmetric force redistribution.

6.3 LIMITATIONS OF THE STUDY AND RECOMMENDATIONS FOR FUTURE RESEARCH

The abutment backfill material was left out of the modelling process for the seismic model. Additionally, no consideration was given to the soil-structure interaction effects for either the abutments or the piers. The foundation is modelled using the assumption that it will be fixed, and this can impact how well the actual seismic response to the structure is modelled.

The confinement reinforcing pier and cap beam are not included in the seismic modelling of the various bridge configurations; therefore, the increased ductility and strength due to confinement during seismic loading are not represented in the model.

Pounding or collision effects in the longitudinal or transverse direction were excluded in the analysis, based on the presence of an existing bridge aligned longitudinally with the bridge, the abutment back wall and web of the cap beam, which restricts relative movement. Furthermore, transverse pounding between the stem of the cap beam due to the skew configuration was not accounted for.

The study did not include epistemic uncertainty in the assessment of the fragility. The probability-based methodology mainly addresses aleatory uncertainty due to random variations in recorded ground motions by statistically accounting for the variation in the cloud analysis. The other types of uncertainty, including model assumptions, the physical properties of materials, representations of damping, structural simplifications, and capacity definitions, have not been quantitatively assessed into the fragility parameters.

6.4 FUTURE RESEARCH DIRECTIONS

The findings and limitations of this research indicate numerous directions for future research. A more comprehensive representation of seismic response can be achieved by incorporating soil-structure interaction (SSI) with flexible foundations into the seismic response of bridges on soft volcanic deposits.

Investigations into new experimental research conducted on unreinforced thin elastomeric pads, particularly with respect to the cyclic shear responses, failure modes, and displacement performance of these pads during bi-directional seismic loadings, are needed to enhance analytical fragility frameworks.

Future investigators need to compare seismic vulnerability using data from both volcanic and tectonic ground motions. This will allow for an evaluation of how different types of earthquakes have different time periods, frequencies, and amounts of load (demand), which can be used to better understand the overall seismic hazard present in this region. Additionally, researchers could also develop hybrid approaches for evaluating seismic vulnerability by combining the analytical work done to date with either observational or experimental data, which would help to lower the amount of epistemic uncertainty present in seismic risk assessments and increase confidence in those evaluations.

REFERENCES

Altieri, D., & Patelli, E. (2020). An efficient approach for computing analytical non-parametric fragility curves. *Structural Safety*, *85*, 101956. https://doi.org/10.1016/j.strusafe.2020.101956

American Association of State Highway and Transportation Officials (Ed.). (2020). *LRFD bridge design specifications* (9th edition). American Association of State Highway and Transportation Officials.

Argyroudis, S., Mitoulis, S., Kaynia, A. M., & Winter, M. G. (2018). Fragility Assessment of Transportation Infrastructure Systems Subjected to Earthquakes. *Geotechnical Earthquake Engineering and Soil Dynamics V*, 174–183. https://doi.org/10.1061/9780784481479.018

Baker, J. W. (2015). Efficient Analytical Fragility Function Fitting Using Dynamic Structural Analysis. *Earthquake Spectra*, *31*(1), 579–599. https://doi.org/10.1193/021113EQS025M

Barajas, A., Journeau, C., Obara, K., & Shapiro, N. M. (2023). Comparison of Continuously Recorded Seismic Wavefields in Tectonic and Volcanic Environments Based on the Network Covariance Matrix. *Journal of*

Geophysical Research: Solid Earth, *128*(12), e2023JB026784. https://doi.org/10.1029/2023JB026784

Bhandari, A. (2023). *Uncertainty Quantification and Fragility Development of Deteriorating RC Bridge Piers* [Master of Science in Civil & Environmental Engineering, Portland State University]. https://doi.org/10.15760/etd.8168

Borzi, B., Ceresa, P., Franchin, P., Noto, F., Calvi, G. M., & Pinto, P. E. (2015a). Seismic Vulnerability of the Italian Roadway Bridge Stock. *Earthquake Spectra*, *31*(4), 2137–2161. https://doi.org/10.1193/070413EQS190M

Borzi, B., Ceresa, P., Franchin, P., Noto, F., Calvi, G. M., & Pinto, P. E. (2015b). Seismic Vulnerability of the Italian Roadway Bridge Stock. *Earthquake Spectra*, *31*(4), 2137–2161. https://doi.org/10.1193/070413EQS190M

Borzi, B., Ceresa, P., Franchin, P., Noto, F., Calvi, G. M., & Pinto, P. E. (2015c). Seismic Vulnerability of the Italian Roadway Bridge Stock. *Earthquake Spectra*, *31*(4), 2137–2161. https://doi.org/10.1193/070413EQS190M

Bridge Deck Behaviour-Hambly. (n.d.).

Brielmaier, A. A., & Hoblitzell, J. R. (n.d.). *NEOPRENE BEARING PADS UNDER REPEATED COMPRESSION AND SHEAR*.

Buratti, N., Minghini, F., Ongaretto, E., Savoia, M., & Tullini, N. (2017). Empirical seismic fragility for the precast RC industrial buildings damaged by the

2012 Emilia (Italy) earthquakes. *Earthquake Engineering & Structural Dynamics*, *46*(14), 2317–2335. https://doi.org/10.1002/eqe.2906

Chang, K.-C., Chang, D.-W., Tsai, M.-H., & Sung, Y.-C. (n.d.). *Seismic Performance of Highway Bridges*.

Chen, W.-F., & Duan, L. (n.d.). *Bridge Engineering Handbook, Second Edition*.

Choe, D.-E., Gardoni, P., Rosowsky, D., & Haukaas, T. (2009). Seismic fragility estimates for reinforced concrete bridges subject to corrosion. *Structural Safety*, *31*(4), 275–283. https://doi.org/10.1016/j.strusafe.2008.10.001

Choi, E., DesRoches, R., & Nielson, B. (2004). Seismic fragility of typical bridges in moderate seismic zones. *Engineering Structures*, *26*(2), 187–199. https://doi.org/10.1016/j.engstruct.2003.09.006

Chopra, A. K., & McKenna, F. (2016). Modeling viscous damping in nonlinear response history analysis of buildings for earthquake excitation. *Earthquake Engineering & Structural Dynamics*, *45*(2), 193–211. https://doi.org/10.1002/eqe.2622

Chopra, A.K. - Dynamics of Structures—Theory and Applications to Earthquake Engineering (4th ed). (n.d.).

Chouw, N., & Hao, H. (2005). Study of SSI and non-uniform ground motion effect on pounding between bridge girders. *Soil Dynamics and Earthquake Engineering*, *25*(7–10), 717–728. https://doi.org/10.1016/j.soildyn.2004.11.015

Contiguglia, C. P., Pelle, A., Briseghella, B., & Nuti, C. (2022). IMPA versus Cloud Analysis and IDA: Different Methods to Evaluate Structural Seismic Fragility. *Applied Sciences*, *12*(7), 3687. https://doi.org/10.3390/app12073687

Cornell, C. A., Jalayer, F., Hamburger, R. O., & Foutch, D. A. (2002). Probabilistic Basis for 2000 SAC Federal Emergency Management Agency Steel Moment Frame Guidelines. *Journal of Structural Engineering*, *128*(4), 526–533. https://doi.org/10.1061/(ASCE)0733-9445(2002)128:4(526)

Cubellis, E., & Marturano, A. (2013). Felt index, source parameters and ground motion evaluation for earthquakes at Mt. Vesuvius. *Annals of Geophysics*, *56*(4), S0439. https://doi.org/10.4401/ag-6445

Deviprasad, B. S., Saseendran, R., & Dodagoudar, G. R. (2022). Fragility analysis of bridge pier supported on rocking shallow foundation under earthquake loading. *Bulletin of Earthquake Engineering*, *20*(12), 6901–6917. https://doi.org/10.1007/s10518-022-01463-3

Di Sarno, L., Da Porto, F., Guerrini, G., Calvi, P. M., Camata, G., & Prota, A. (2019). Seismic performance of bridges during the 2016 Central Italy earthquakes. *Bulletin of Earthquake Engineering*, *17*(10), 5729–5761. https://doi.org/10.1007/s10518-018-0419-4

Feng, R., Wang, X., Yuan, W., & Yu, J. (2018). Impact of seismic excitation direction on the fragility analysis of horizontally curved concrete bridges. *Bulletin*

of Earthquake Engineering, *16*(10), 4705–4733. https://doi.org/10.1007/s10518-018-0400-2

Forcellini, D., & Alzabeebee, S. (2023). Seismic fragility assessment of geotechnical seismic isolation (GSI) for bridge configuration. *Bulletin of Earthquake Engineering*, *21*(8), 3969–3990. https://doi.org/10.1007/s10518-022-01356-5

Franchin, P., Lupoi, A., Noto, F., & Tesfamariam, S. (2016). Seismic fragility of reinforced concrete girder bridges using Bayesian belief network. *Earthquake Engineering & Structural Dynamics*, *45*(1), 29–44. https://doi.org/10.1002/eqe.2613

Fu, X., Guo, D., Li, G., Li, H., & Zhu, D. (2024). Seismic vulnerability assessment of electrical substation system based on the hybrid fragility functions and Bayesian network. *Earthquake Engineering & Structural Dynamics*, eqe.4219. https://doi.org/10.1002/eqe.4219

Gardoni, P., Mosalam, K. M., & Kiureghian, A. D. (2003). PROBABILISTIC SEISMIC DEMAND MODELS AND FRAGILITY ESTIMATES FOR RC BRIDGES. *Journal of Earthquake Engineering*, *7*(sup001), 79–106. https://doi.org/10.1080/13632460309350474

Gauron, O., Saidou, A., Busson, A., Siqueira, G. H., & Paultre, P. (2018). Experimental determination of the lateral stability and shear failure limit

states of bridge rubber bearings. *Engineering Structures*, *174*, 39–48. https://doi.org/10.1016/j.engstruct.2018.07.039

Han, Q., Du, X., Liu, J., Li, Z., Li, L., & Zhao, J. (2009). Seismic damage of highway bridges during the 2008 Wenchuan earthquake. *Earthquake Engineering and Engineering Vibration*, *8*(2), 263–273. https://doi.org/10.1007/s11803-009-8162-0

Hazus Earthquake Model Technical Manual. (n.d.).

Htay, K. T., Tanjung, J., Masrilayanti, Olivia, M., Mohamed Nazri, F., & Bur, M. (2024). A Proposed Fragility Curve Based on PO-ID Hybrid Analysis for Seismic Assessment Performance of the Reinforced Concrete Continuous Bridges in Earthquake Prone Area. *Buildings*, *14*(12), 3875. https://doi.org/10.3390/buildings14123875

Iqbal, W., & Head, M. (2024). Parametric study for shear failure of bearing pads due to hurricane-induced wave loadings. *Advances in Bridge Engineering*, *5*(1), 30. https://doi.org/10.1186/s43251-024-00138-0

Jalayer, F., Carozza, S., De Risi, R., Manfredi, G., & Mbuya, E. (2016). Performance-based flood safety-checking for non-engineered masonry structures. *Engineering Structures*, *106*, 109–123. https://doi.org/10.1016/j.engstruct.2015.10.007

Jeon, J.-S., DesRoches, R., Kim, T., & Choi, E. (2016). Geometric parameters affecting seismic fragilities of curved multi-frame concrete box-girder

bridges with integral abutments. *Engineering Structures*, *122*, 121–143. https://doi.org/10.1016/j.engstruct.2016.04.037

Karamlou, A., & Bocchini, P. (2015). Computation of bridge seismic fragility by large-scale simulation for probabilistic resilience analysis. *Earthquake Engineering & Structural Dynamics*, *44*(12), 1959–1978. https://doi.org/10.1002/eqe.2567

Kawashima, K., Takahashi, Y., Ge, H., Wu, Z., & Zhang, J. (2009). DAMAGE OF BRIDGES IN 2008 WENCHUAN, CHINA EARTHQUAKE. *Doboku Gakkai Ronbunshuu A*, *65*(3), 825–843. https://doi.org/10.2208/jsceja.65.825

Khurshid, F. B., Izhar, M. S., Islam, N., Khan, N. A., & Khan, M. B. (2025). Seismic Fragility of Fixed and Flexible Base RC Bridge under Near-Fault Directivity Effects. *Journal of the Civil Engineering Forum*, 53–74. https://doi.org/10.22146/jcef.22631

Lallemant, D., Kiremidjian, A., & Burton, H. (2015a). Statistical procedures for developing earthquake damage fragility curves. *Earthquake Engineering & Structural Dynamics*, *44*(9), 1373–1389. https://doi.org/10.1002/eqe.2522

Lallemant, D., Kiremidjian, A., & Burton, H. (2015b). Statistical procedures for developing earthquake damage fragility curves. *Earthquake Engineering & Structural Dynamics*, *44*(9), 1373–1389. https://doi.org/10.1002/eqe.2522

Lapins, S., Roman, D. C., Rougier, J., De Angelis, S., Cashman, K. V., & Kendall, J.-M. (2020). An examination of the continuous wavelet transform for volcano-seismic spectral analysis. *Journal of Volcanology and Geothermal Research*, *389*, 106728. https://doi.org/10.1016/j.jvolgeores.2019.106728

Lavezzo, D. (2022). The Genoa Decree and Normative Acts Adopted after the Collapse of the Morandi Bridge in an Economic Perspective. *Polish Journal of Political Science*, 45–61. https://doi.org/10.58183/pjps.04012022

Li, H., Li, L., Zhou, G., & Xu, L. (2020). Effects of various modeling uncertainty parameters on the seismic response and seismic fragility estimates of the aging highway bridges. *Bulletin of Earthquake Engineering*, *18*(14), 6337–6373. https://doi.org/10.1007/s10518-020-00934-9

Lin, C.-C. J., Hung, H.-H., Liu, K.-Y., & Chai, J.-F. (2010). Reconnaissance Observation on Bridge Damage Caused by the 2008 Wenchuan (China) Earthquake. *Earthquake Spectra*, *26*(4), 1057–1083. https://doi.org/10.1193/1.3479947

Lu, C.-H., Liu, K.-Y., & Chang, K.-C. (2011). Seismic performance of bridges with rubber bearings: Lessons learnt from the 1999 Chi-Chi Taiwan earthquake. *Journal of the Chinese Institute of Engineers*, *34*(7), 889–904. https://doi.org/10.1080/02533839.2011.591920

Lyu, M., Feng, D., Cao, X., & Beer, M. (2024). A full-probabilistic cloud analysis for structural seismic fragility via decoupled M-PDEM. *Earthquake*

Engineering & Structural Dynamics, *53*(5), 1863–1881. https://doi.org/10.1002/eqe.4093

M. J. N. Priestley, F. Seible, G. M. Calvi-Seismic Design and Retrofit of Bridges, Wiley-Interscience (1996) (1). (n.d.).

Mangalathu, S., Jeon, J.-S., Padgett, J. E., & DesRoches, R. (2016). ANCOVA-based grouping of bridge classes for seismic fragility assessment. *Engineering Structures*, *123*, 379–394. https://doi.org/10.1016/j.engstruct.2016.05.054

Minnucci, L., Scozzese, F., Carbonari, S., Gara, F., & Dall'Asta, A. (2022). Innovative Fragility-Based Method for Failure Mechanisms and Damage Extension Analysis of Bridges. *Infrastructures*, *7*(9), 122. https://doi.org/10.3390/infrastructures7090122

Muntasir Billah, A. H. M., & Shahria Alam, M. (2015). Seismic fragility assessment of highway bridges: A state-of-the-art review. *Structure and Infrastructure Engineering*, *11*(6), 804–832. https://doi.org/10.1080/15732479.2014.912243

Nappi, R., Porfido, S., Paganini, E., Vezzoli, L., Ferrario, M. F., Gaudiosi, G., Alessio, G., & Michetti, A. M. (2021). The 2017, MD = 4.0, Casamicciola Earthquake: ESI-07 Scale Evaluation and Implications for the Source Model. *Geosciences*, *11*(2), 44. https://doi.org/10.3390/geosciences11020044

Nielson, B. G., & DesRoches, R. (2007a). Analytical Seismic Fragility Curves for Typical Bridges in the Central and Southeastern United States. *Earthquake Spectra*, *23*(3), 615–633. https://doi.org/10.1193/1.2756815

Nielson, B. G., & DesRoches, R. (2007b). Analytical Seismic Fragility Curves for Typical Bridges in the Central and Southeastern United States. *Earthquake Spectra*, *23*(3), 615–633. https://doi.org/10.1193/1.2756815

Nielson, B. G., & DesRoches, R. (2007c). Seismic fragility methodology for highway bridges using a component level approach. *Earthquake Engineering & Structural Dynamics*, *36*(6), 823–839. https://doi.org/10.1002/eqe.655

Noori, H. R., Memarpour, M. M., Yakhchalian, M., & Soltanieh, S. (2019a). Effects of ground motion directionality on seismic behavior of skewed bridges considering SSI. *Soil Dynamics and Earthquake Engineering*, *127*, 105820. https://doi.org/10.1016/j.soildyn.2019.105820

Noori, H. R., Memarpour, M. M., Yakhchalian, M., & Soltanieh, S. (2019b). Effects of ground motion directionality on seismic behavior of skewed bridges considering SSI. *Soil Dynamics and Earthquake Engineering*, *127*, 105820. https://doi.org/10.1016/j.soildyn.2019.105820

Nunziata, C., & Vaccari, F. (n.d.-a). *Seismic Ground Motion Expected for the Eastern District of Naples*.

Nunziata, C., & Vaccari, F. (n.d.-b). *Seismic Ground Motion Expected for the Eastern District of Naples*.

Ozell, A. M., & Diniz, J. F. (n.d.). *Report on Tests of Neoprene Pads Under Repeated Shear Loads*.

Ozsarac, V., Furinghetti, M., & Monteiro, R. (2023). Seismic risk assessment of ageing existing reinforced concrete bridges accounting for uncertainty in bearing properties. *Engineering Structures*, *293*, 116730. https://doi.org/10.1016/j.engstruct.2023.116730

Pang, Y., Wei, K., Wang, J., & Zhang, S. (2023). An efficient and accurate fragility approach for seismic performance assessment of structures. *Earthquake Engineering and Resilience*, *2*(4), 403–417. https://doi.org/10.1002/eer2.64

Perdomo, C., Monteiro, R., & Sucuoğlu, H. (2022). Development of Fragility Curves for Single-Column RC Italian Bridges Using Nonlinear Static Analysis. *Journal of Earthquake Engineering*, *26*(5), 2328–2352. https://doi.org/10.1080/13632469.2020.1760153

Petrini, L., Maggi, C., Priestley, M. J. N., & Calvi, G. M. (2008). Experimental Verification of Viscous Damping Modeling for Inelastic Time History Analyzes. *Journal of Earthquake Engineering*, *12*(sup1), 125–145. https://doi.org/10.1080/13632460801925822

Pinzón, L. A., Hidalgo-Leiva, D. A., & Pujades, L. G. (2024). Correction Factors to Account for Seismic Directionality Effects: Case Study of the Costa Rican Strong Motion Database. *Geosciences*, *14*(5), 139. https://doi.org/10.3390/geosciences14050139

Priestley et al, 1996. (n.d.).

Priestley, M. J. N., & Grant, D. N. (2005). VISCOUS DAMPING IN SEISMIC DESIGN AND ANALYSIS. *Journal of Earthquake Engineering*, *9*(sup2), 229–255. https://doi.org/10.1142/S1363246905002365

Priestley, M. J. N., & Kowalsky, M. J. (1998). Aspects of drift and ductility capacity of rectangular cantilever structural walls. *Bulletin of the New Zealand Society for Earthquake Engineering*, *31*(2), 73–85. https://doi.org/10.5459/bnzsee.31.2.73-85

Ramanathan, K., Padgett, J. E., & DesRoches, R. (2015a). Temporal evolution of seismic fragility curves for concrete box-girder bridges in California. *Engineering Structures*, *97*, 29–46. https://doi.org/10.1016/j.engstruct.2015.03.069

Ramanathan, K., Padgett, J. E., & DesRoches, R. (2015b). Temporal evolution of seismic fragility curves for concrete box-girder bridges in California. *Engineering Structures*, *97*, 29–46. https://doi.org/10.1016/j.engstruct.2015.03.069

Ramanathan, K., Padgett, J. E., & DesRoches, R. (2015c). Temporal evolution of seismic fragility curves for concrete box-girder bridges in California. *Engineering Structures*, *97*, 29–46. https://doi.org/10.1016/j.engstruct.2015.03.069

Rolandi, G., Troise, C., Sacchi, M., Di Lascio, M., & De Natale, G. (2025). The 1538 eruption at the Campi Flegrei resurgent caldera: Implications for future unrest and eruptive scenarios. *Natural Hazards and Earth System Sciences*, *25*(9), 3421–3453. https://doi.org/10.5194/nhess-25-3421-2025

Santarsiero, G., Masi, A., Picciano, V., & Digrisolo, A. (2021). The Italian Guidelines on Risk Classification and Management of Bridges: Applications and Remarks on Large Scale Risk Assessments. *Infrastructures*, *6*(8), 111. https://doi.org/10.3390/infrastructures6080111

Sarkis, A. I., Palermo, A., Kammouh, O., & Cimellaro, G. P. (2018). Seismic resilience of road bridges: Lessons learned from the 14 November 2016 Kaikōura Earthquake. In N. Powers, D. M. Frangopol, R. Al-Mahaidi, & C. Caprani (Eds.), *Maintenance, Safety, Risk, Management and Life-Cycle Performance of Bridges* (1st ed., pp. 1988–1995). CRC Press. https://doi.org/10.1201/9781315189390-271

Satyanarayana, A., Sindura, V., Geetha, L., Kumar, R., Shah, M. A., & Christo, M. S. (2025). A multifaceted comparative analysis of incremental dynamic and

static pushover methods in bridge structural assessment, integrated with artificial neural network and genetic algorithm approach. *Discover Materials*, *5*(1), 84. https://doi.org/10.1007/s43939-025-00262-2

Scala, A., Niero, L., Brezzi, L., Gabrieli, F., Gibin, F., Pellegrino, C., Simonini, P., Sarhosis, V., & Zampieri, P. (2025). Extreme natural events and bridge collapses: Statistical insights in Italy. *International Journal of Disaster Risk Reduction*, *131*, 105880. https://doi.org/10.1016/j.ijdrr.2025.105880

Scandone, R., Giacomelli, L., & Gasparini, P. (1993). Mount Vesuvius: 2000 years of volcanological observations. *Journal of Volcanology and Geothermal Research*, *58*(1–4), 5–25. https://doi.org/10.1016/0377-0273(93)90099-D

Scawthorn, C., & Porter, K. A. (2011). *Aspects of the 11 March 2011 Eastern Japan Earthquake and Tsunami*.

Shabani, A., & Kioumarsi, M. (2023). Seismic assessment and strengthening of a historical masonry bridge considering soil-structure interaction. *Engineering Structures*, *293*, 116589. https://doi.org/10.1016/j.engstruct.2023.116589

Shuler, A., Ekström, G., & Nettles, M. (2013). Physical mechanisms for vertical-CLVD earthquakes at active volcanoes. *Journal of Geophysical Research: Solid Earth*, *118*(4), 1569–1586. https://doi.org/10.1002/jgrb.50131

Silva, V., Akkar, S., Baker, J., Bazzurro, P., Castro, J. M., Crowley, H., Dolsek, M., Galasso, C., Lagomarsino, S., Monteiro, R., Perrone, D., Pitilakis, K., & Vamvatsikos, D. (2019). Current Challenges and Future Trends in Analytical Fragility and Vulnerability Modeling. *Earthquake Spectra*, *35*(4), 1927–1952. https://doi.org/10.1193/042418EQS101O

Song, S., Xie, Y., Wang, Y., Zhang, W., Kurtulus, A., Apaydin, N. M., & Taciroglu, E. (2024). Seismic fragility and vulnerability assessment of a multi-span irregular curved bridge under spatially varying ground motions. *Soil Dynamics and Earthquake Engineering*, *180*, 108585. https://doi.org/10.1016/j.soildyn.2024.108585

Stefanidou, S. P., & Kappos, A. J. (2019). Bridge-specific fragility analysis: When is it really necessary? *Bulletin of Earthquake Engineering*, *17*(4), 2245–2280. https://doi.org/10.1007/s10518-018-00525-9

Straub, D., & Der Kiureghian, A. (2008). Improved seismic fragility modeling from empirical data. *Structural Safety*, *30*(4), 320–336. https://doi.org/10.1016/j.strusafe.2007.05.004

Tekeste, G. G., Correia, A. A., & Costa, A. G. (2023). Bayesian updating of seismic fragility curves through experimental tests. *Bulletin of Earthquake Engineering*, *21*(4), 1943–1976. https://doi.org/10.1007/s10518-022-01589-4

Thakkar, K., Rana, A., & Goyal, H. (2023). Fragility analysis of bridge structures: A global perspective & critical review of past & present trends. *Advances in Bridge Engineering*, *4*(1), 10. https://doi.org/10.1186/s43251-023-00089-y

Wang, P., Han, Q., & Du, X. (2014). Seismic performance of circular RC bridge columns with flexure–torsion interaction. *Soil Dynamics and Earthquake Engineering*, *66*, 13–30. https://doi.org/10.1016/j.soildyn.2014.06.028

Wang, X., Ye, A., & Ji, B. (2019). Fragility-based sensitivity analysis on the seismic performance of pile-group-supported bridges in liquefiable ground undergoing scour potentials. *Engineering Structures*, *198*, 109427. https://doi.org/10.1016/j.engstruct.2019.109427

Wu, F., Zhou, J., Zhao, Y., Wang, G., Tang, W., Luo, J., Ibrahim, U., & Meng, Y. (2021). Performance-Based Seismic Fragility and Risk Assessment of Five-Span Continuous Rigid Frame Bridges. *Advances in Civil Engineering*, *2021*(1), 6657663. https://doi.org/10.1155/2021/6657663

Xie, Y., & DesRoches, R. (2019). Sensitivity of seismic demands and fragility estimates of a typical California highway bridge to uncertainties in its soil-structure interaction modeling. *Engineering Structures*, *189*, 605–617. https://doi.org/10.1016/j.engstruct.2019.03.115

Yang, C. S., DesRoches, R., & Padgett, J. E. (2009). Fragility Curves for a Typical California Box Girder Bridge. *TCLEE 2009*, 1–12. https://doi.org/10.1061/41050(357)5

Yang, H. Z., & Koh, C. G. (2021). Seismic Risk Evaluation by Fragility Curves Using Metamodel Methods. In L. Gelman, N. Martin, A. A. Malcolm, & C. K. (Edmund) Liew (Eds.), *Advances in Condition Monitoring and Structural Health Monitoring* (pp. 313–323). Springer Singapore. https://doi.org/10.1007/978-981-15-9199-0_29

Zhang, Y., Fan, J., & Fan, W. (2016). Seismic fragility analysis of concrete bridge piers reinforced by steel fibers. *Advances in Structural Engineering*, *19*(5), 837–848. https://doi.org/10.1177/1369433216630440

Zhao, Y., Hu, H., Bai, L., Tang, M., Chen, H., & Su, D. (2021). Fragility Analyses of Bridge Structures Using the Logarithmic Piecewise Function-Based Probabilistic Seismic Demand Model. *Sustainability*, *13*(14), 7814. https://doi.org/10.3390/su13147814

Zhou, Y., Gao, C., Yang, S., Guo, W., & Jiang, L. (2024). Seismic Fragility Analysis of Reinforced Concrete Simply Supported Girder Bridges Resting on Double-Column Piers for High Speed Railway. *Buildings*, *14*(10), 3072. https://doi.org/10.3390/buildings14103072

Zhuang, L., & Pang, Y. (2021). *Enhanced Cloud Method (E-Cloud) for Efficient Seismic Fragility Assessment of Structures*. In Review. https://doi.org/10.21203/rs.3.rs-647920/v1

APPENDIX A. Validation of the Gravity Analysis for the Three Cases

i) Fundamenta Natural Periods

Table A. 1. Comparison of Modal Periods Between OpenSees and MIDAS for CASE-1

Mode Number	Mode Shape Characterised	OpenSees	MIDAS	Relative OpenSees Midas Discrepancy
1	Full-bridge longitudinal	0.6423	0.6910	7.04%
2	Full-bridge Transversal	0.1035	0.1029	-0.55%
3	Full-bridge Torsional mode, anti-symmetric Transversal displacement	0.0482	0.0479	-0.57%
4	Full-bridge Torsional mode, anti-symmetric longitudinal displacement	0.0315	0.0313	-0.66%

Table A. 2. Comparison of Modal Periods Between OpenSees and MIDAS for CASE-2

Mode Number	Mode Shape Characterised	OpenSees	MIDAS	Relative OpenSees Midas Discrepancy
1	Full-bridge longitudinal	0.9742	0.9885	1.44%
2	Full-bridge Transversal	0.8561	0.8533	-0.32%
3	Full-bridge Torsional mode, anti-symmetric Transversal displacement	0.8420	0.8418	-0.02%
4	Full-bridge Torsional mode, anti-symmetric longitudinal displacement	0.8396	0.8395	-0.01%

ii) Support Reaction Forces Under Gravity Loads

Table A. 3. Support Reaction Forces Between OpenSees and MIDAS for CASE-1

Location/Reaction	FX (kN)	FY (kN)	FY (kN)	MX (KN.m)	MY (KN.m)	MZ (Kn.m)
Abutment-MIDAS	0.000	0.000	1284.346	0.000	0.000	0.000
Abutment-OpenSees	0.000	0.000	1281.290	0.000	0.000	0.000
Pier-MIDAS	0.000	0.000	5176.409	0.000	0.000	0.000
Pier-OpenSees	0.000	0.000	5182.530	0.000	0.000	0.000

Table A. 4. Support Reaction Forces Between OpenSees and MIDAS for CASE-2

Location/Reaction	FX (kN)	FY (kN)	FY (kN)	MX (KN.m)	MY (KN.m)	MZ (Kn.m)
Abutment-MIDAS	10.239	0.000	1678.050	0.000	10.495	0.000
Abutment-OpenSees	10.239	0.000	1678.050	0.000	10.495	0.000
Pier-MIDAS	0.000	0.000	4185.600	0.000	0.000	0.000
Pier-OpenSees	0.000	0.000	4185.600	0.000	0.000	0.000

iii) Nodal Displacements and Deformations Under Gravity Loads.

Table A. 5. Nodal Displacements and Deformations for Case-1

Location	D_X-(mm)	D_Y-(mm)	D_Z-(mm)
Mid-CapBeam-MIDAS	0.000	0.000	-0.814
Mid-CapBeam-OpenSees	0.000	0.000	-0.904
Top Column-MIDAS	0.000	-0.002	-0.585
Top Column -OpenSees	0.000	-0.108	-0.489

Table A. 6. Nodal Displacements and Deformations for Case-2

Location	D_X-(mm)	D_Y-(mm)	D_Z-(mm)
Mid-CapBeam-MIDAS	0.000	0.000	-0.685
Mid-CapBeam-OpenSees	0.000	0.000	-0.762
Top Column-MIDAS	0.000	0.001	-0.473
Top Column -OpenSees	0.000	-0.184	-0.394

Table A. 7. Nodal Displacements and Deformations for Case-3.

Location	D_X-(mm)	D_Y-(mm)	D_Z-(mm)
Mid-CapBeam-MIDAS	0.000	0.000	-0.747
Mid-CapBeam-OpenSees	0.001	0.005	-0.910
Top Column-MIDAS	0.010	0.004	-0.473
Top Column -OpenSees	0.155	0.192	-0.393

APPENDIX B. Validation of the Response History Results for the Three Cases

i) Longitudinal Force and Displacement Response at the Top Pier

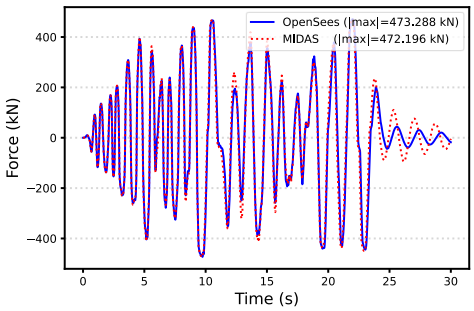

(a-1) (Case-1)

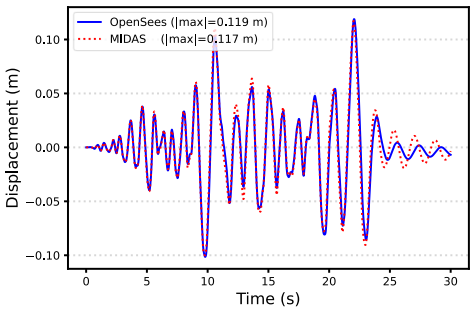

(b-1) (Case1)

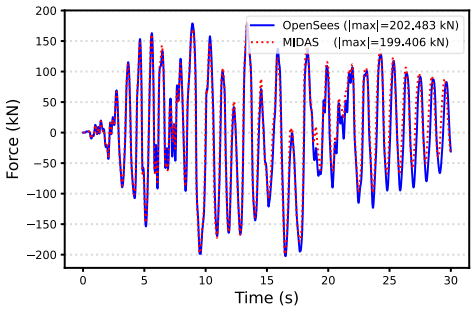

(a-2) (Case-2)

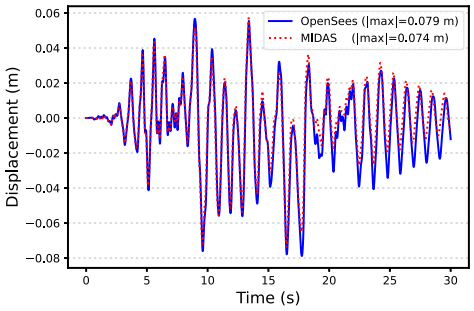

(b-2) (Case-2)

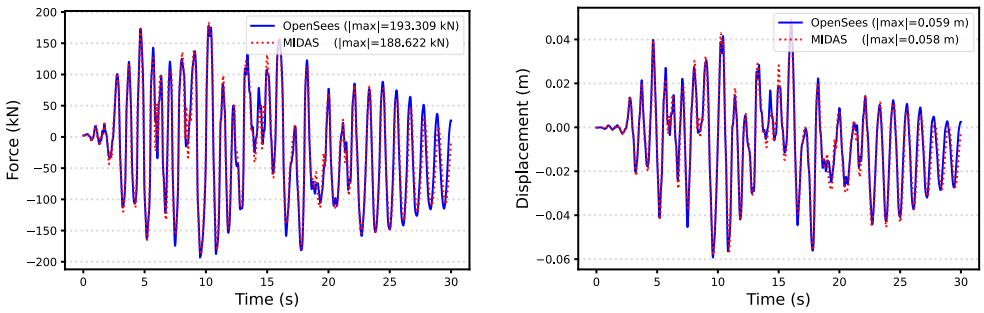

(a-3) (Case-3) (b-3) (Case-3)

Figure B. 1. (a-1, 2, 3) Longitudinal forces at the top of the pier for the three cases are shown sequentially, (b-1, 2, 3) Longitudinal displacement at the top of the pier for the three cases, presented in order

ii) Transversal Force and Displacement Response at the Top Pier

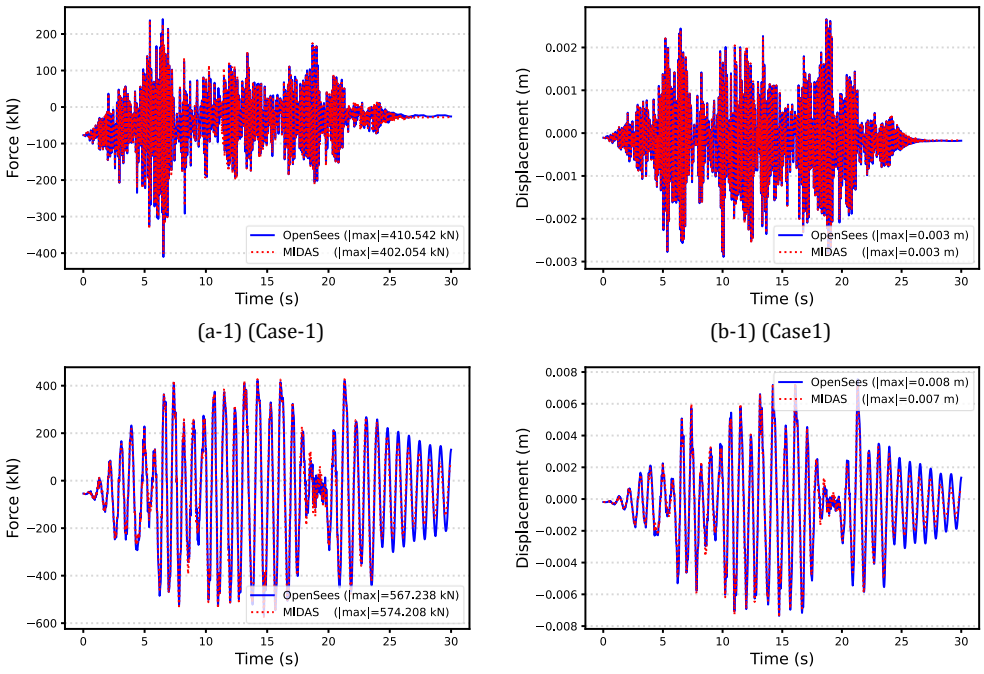

(a-1) (Case-1) (b-1) (Case1)

(a-2) (Case-2) (b-2) (Case-2)

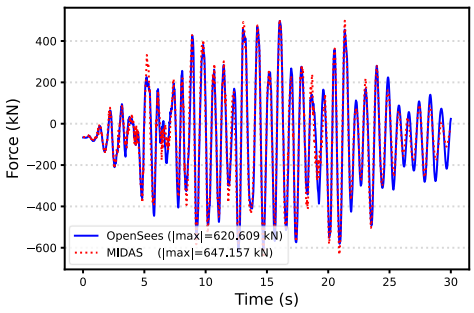

(a-3) (Case-3)

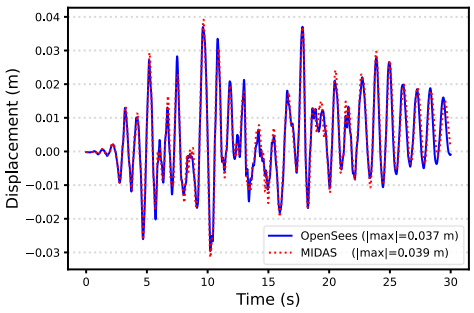

(b-3) (Case-3)

Figure B. 2. (a-1, 2, 3) Transversal forces at the top of the pier for the three cases are shown sequentially, (b-1, 2, 3) Transversal displacement at the top of the pier for the three cases, presented in order

iii) Moment-Curvature Response for Piers

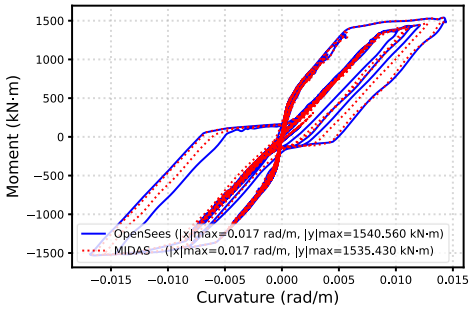

(a-1) (Case-1)

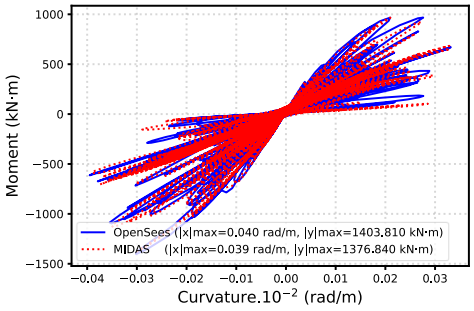

(b-1) (Case-1)

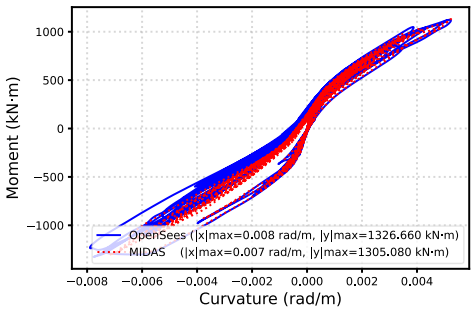

(a-2) (Case-2)

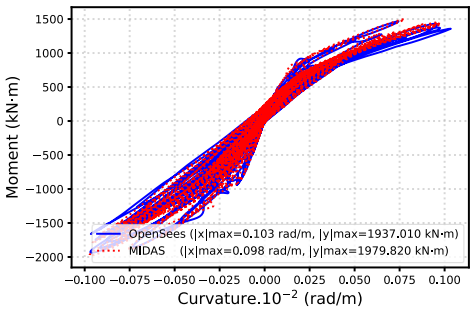

(b-2) (Case-2)

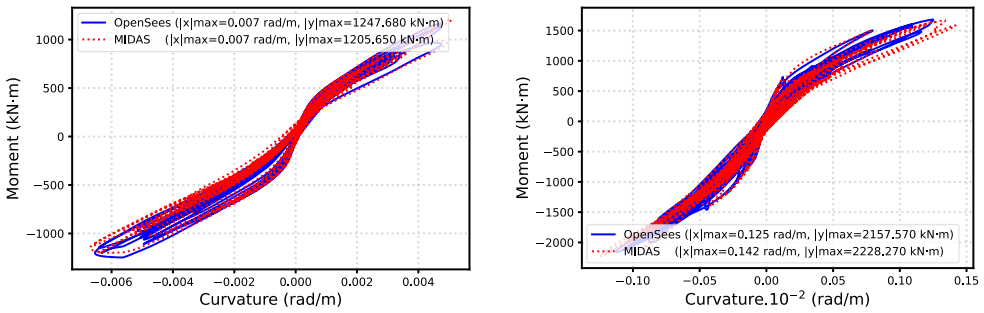

(a-3) (case-3) (b-3) (case-3)

Figure B. 3. (a-1,2,3) Longitudinal moment-curvature at the base of the pier for the three cases, presented sequentially. (b-1,2,3) Transversal moment-curvature at the base of the pier for the three cases, presented sequentially

iv) Moment-Curvature Response for Cap-Beams

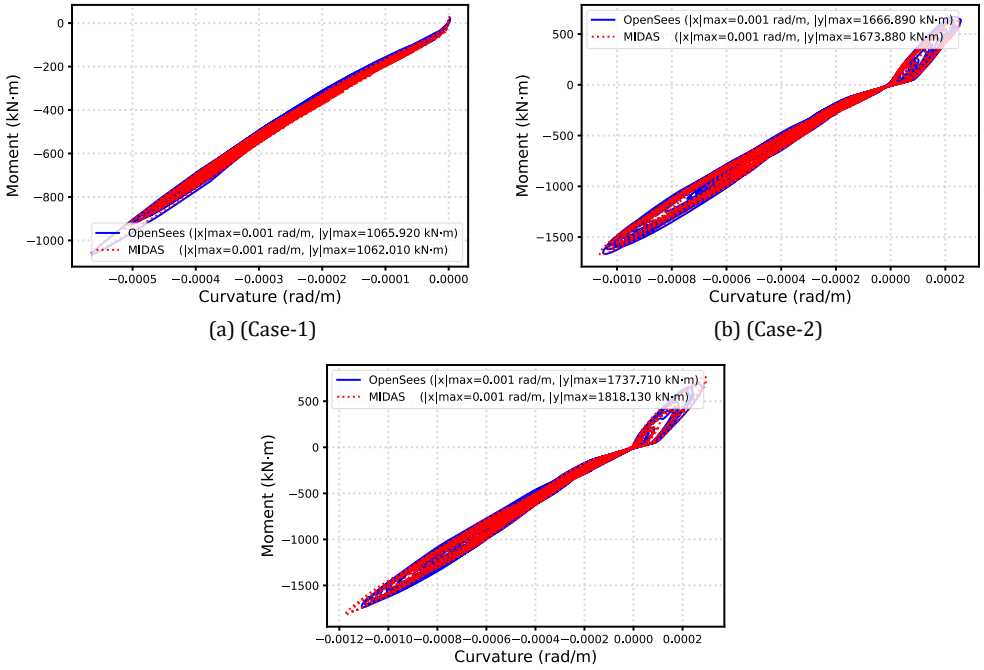

(a) (Case-1) (b) (Case-2)

(c) (Case-3)

Figure B. 4. Moment-curvature response about the Y-axis for the cap beam (a) Case 1, (b) Case-2, (c) Case-3

v) *Longitudinal Force-Displacement Response of Elastomeric Pad Bearing (EPB-29, as shown in Figure 3-2)*

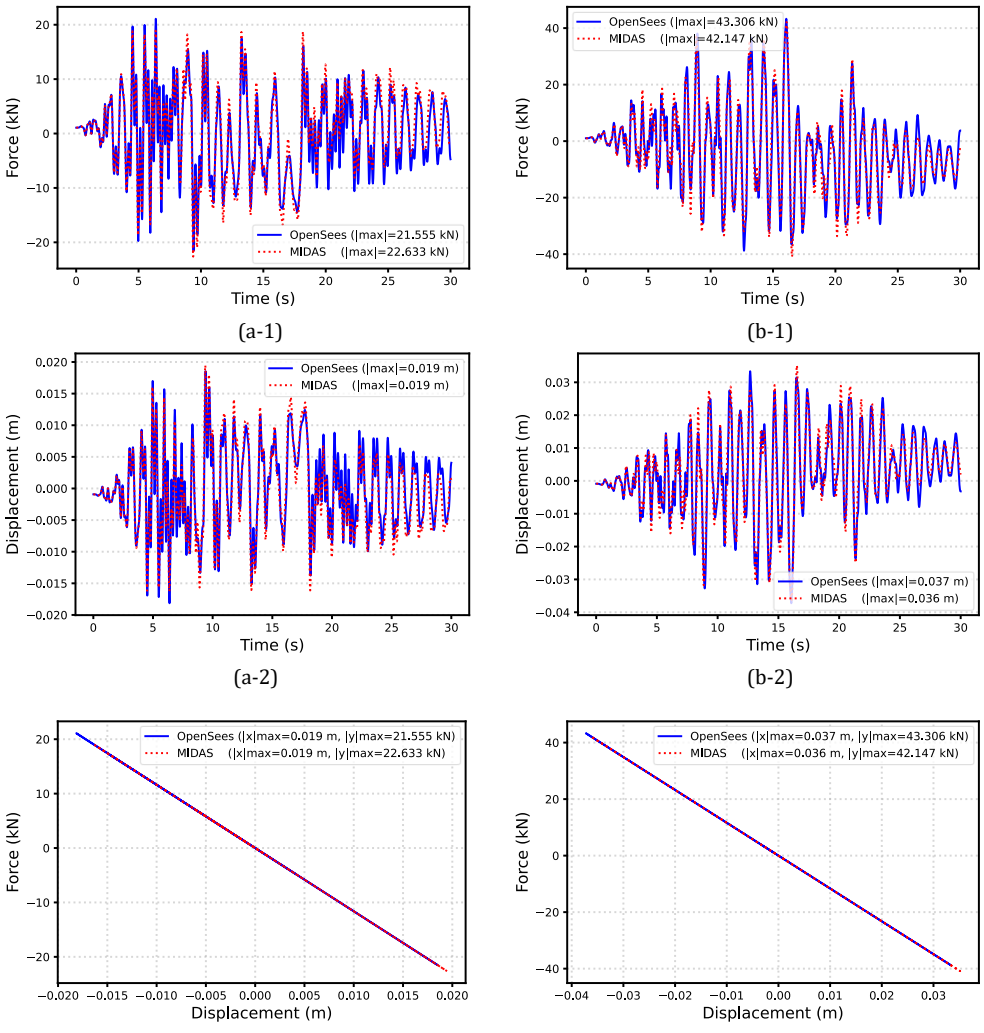

Figure B. 5. (a-1,2,3) longitudinal force-displacement relationship for the bearing in Case-2; corresponding results for Case-3 (b-1,2,3)

vi) Transverse Force-Displacement Response of Elastomeric Pad Bearing (EPB-29, as shown in Figure 3-2)

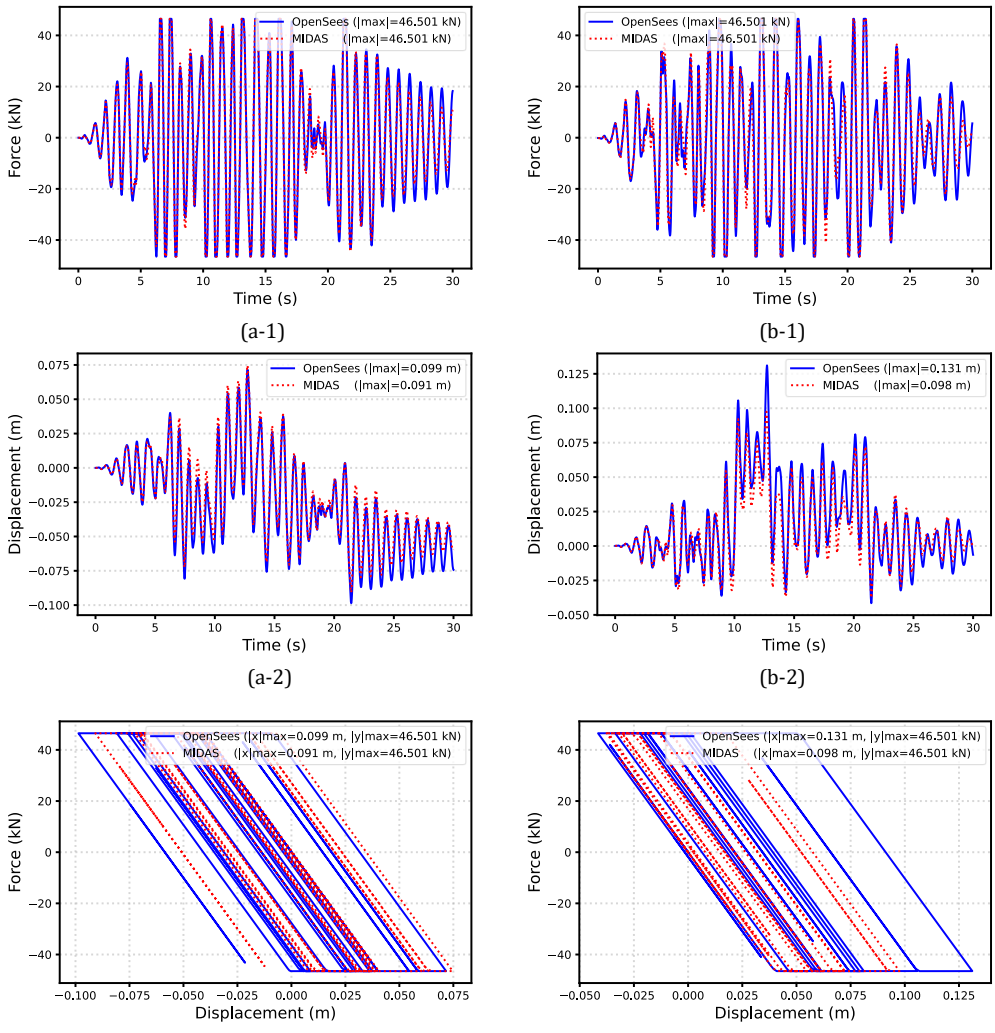

Figure B. 6. (a-1,2,3) Transversal force-displacement relationship for the bearing in Case-2; corresponding results for Case-3 (b-1,2,3)

APPENDIX C. Fragility-based Regression

i) Cloud analysis for the cap beam in each friction case

The regression-based DCR-PGAgeo relationships show similar demand trends across all damage states. Regarding the skewed (30 degrees) case, the DCR value was slightly higher than that associated with the orthogonal configuration, indicating that the skew capbeam is somewhat more vulnerable.

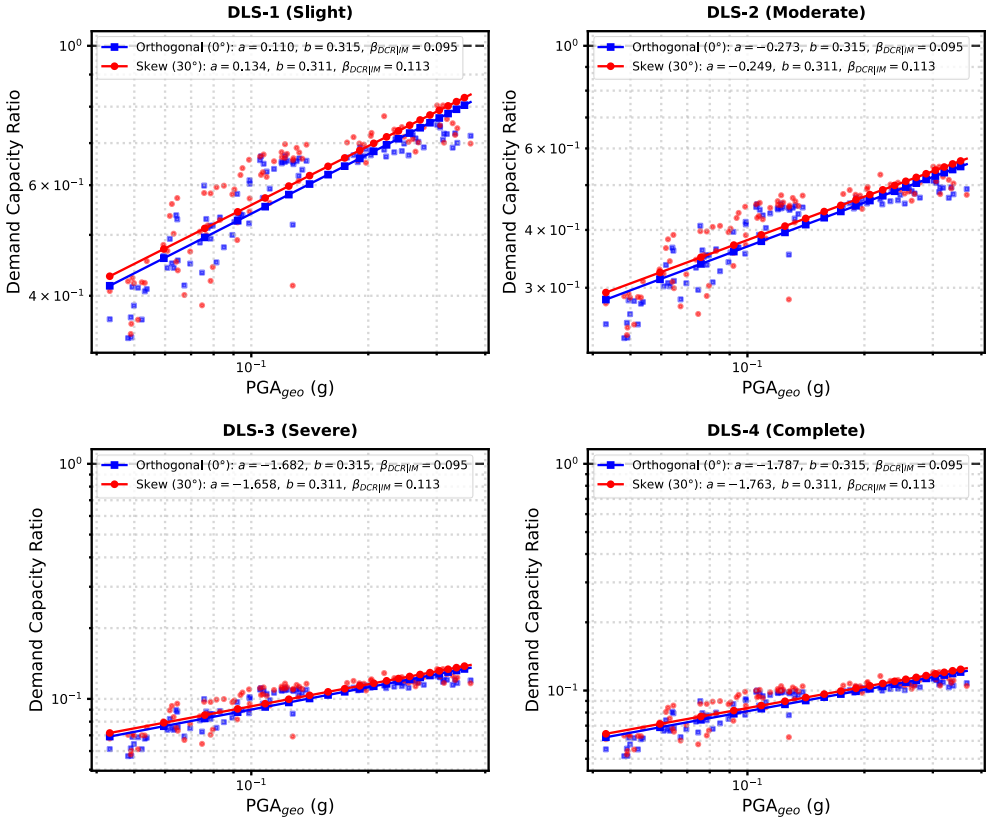

Figure C. 1. Regression-based probabilistic seismic (DCR) and (PGA_{geo}) analysis for the capbeam in the two friction cases

ii) Cloud analysis for the critical Bearing in each friction case

The regression analysis of the critical bearing presented is consistent with the trend with respect to the DCR against PGA_{geo}. Furthermore, the higher demand in the skewed case is driven by global geometric coupling effects, not by differences

in bearing properties, as the local bearing axes and constitutive behaviour remain the same in both configurations.

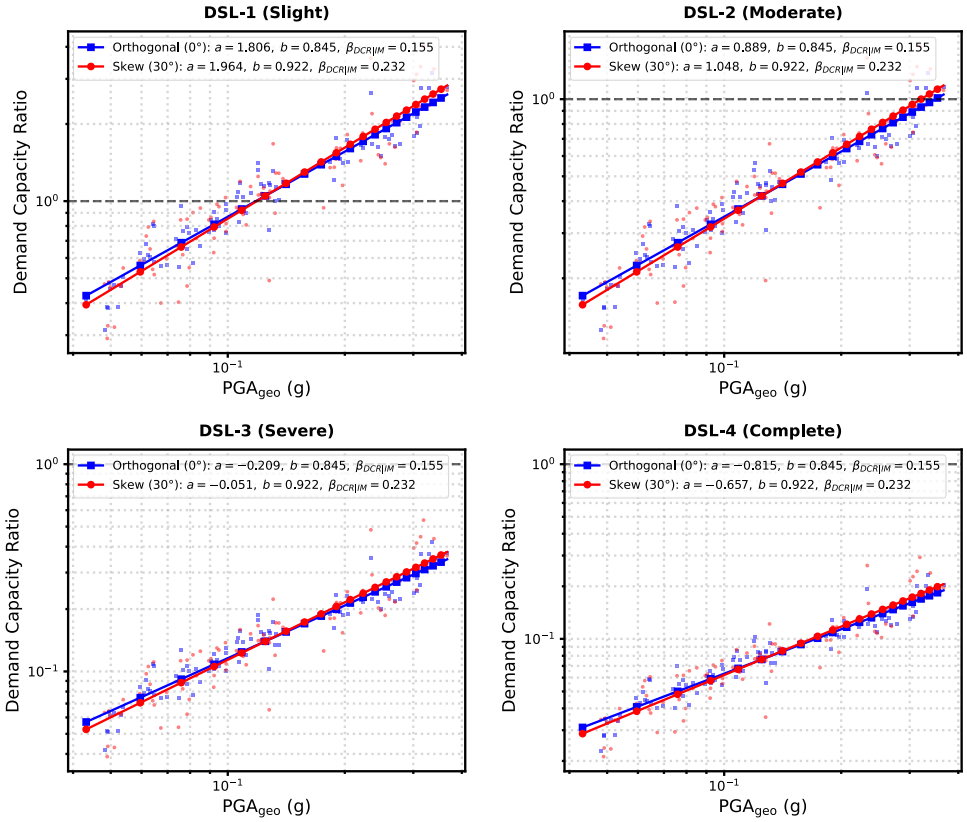

Figure C. 2. Regression-based probabilistic seismic (DCR) and (PGA_{geo}) analysis for the critical bearing over the piers in the two friction cases

iii) Fragility based on cloud analysis for the global Case 1 (fixed pier bridge)

The Figure C. 5 analyses the cloud for the global fixed pier bridge. The Demand Capacity Ratio (DCR) uses a series system approach, where the maximum demand between the pier and cap beam controls the response. The resulting fragility curves estimate exceedance probability and system-level seismic vulnerability, as shown in Figure C. 4.

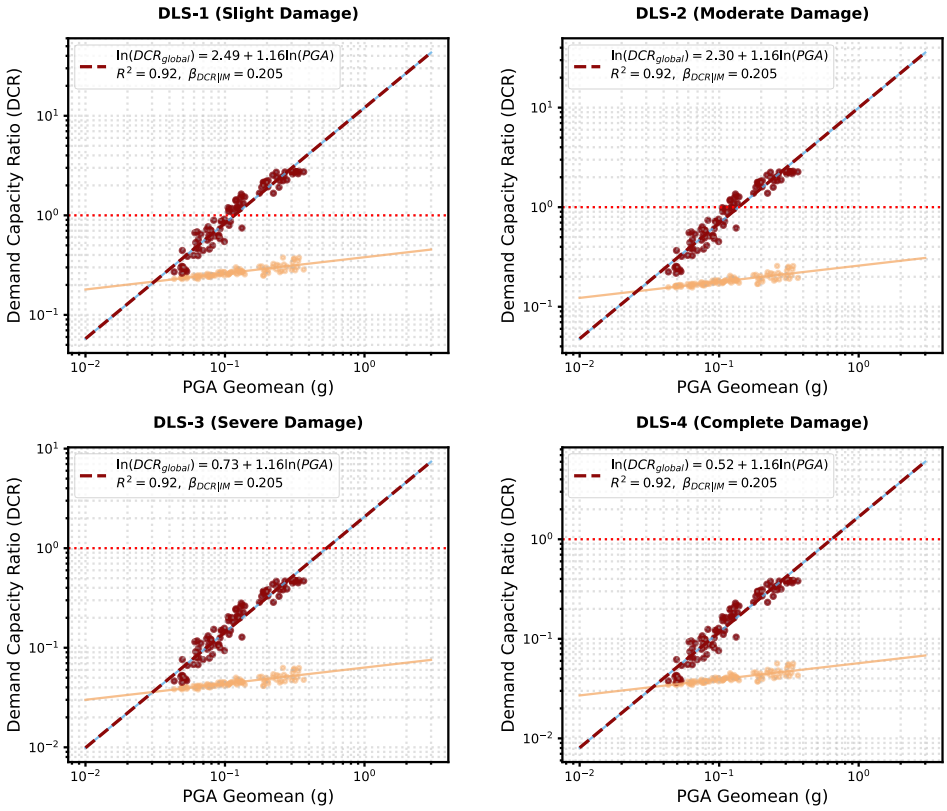

Figure C. 3. Regression-based probabilistic seismic (DCR) against (PGA_{geo}) analysis for compenent and the global fixed-pier bridge

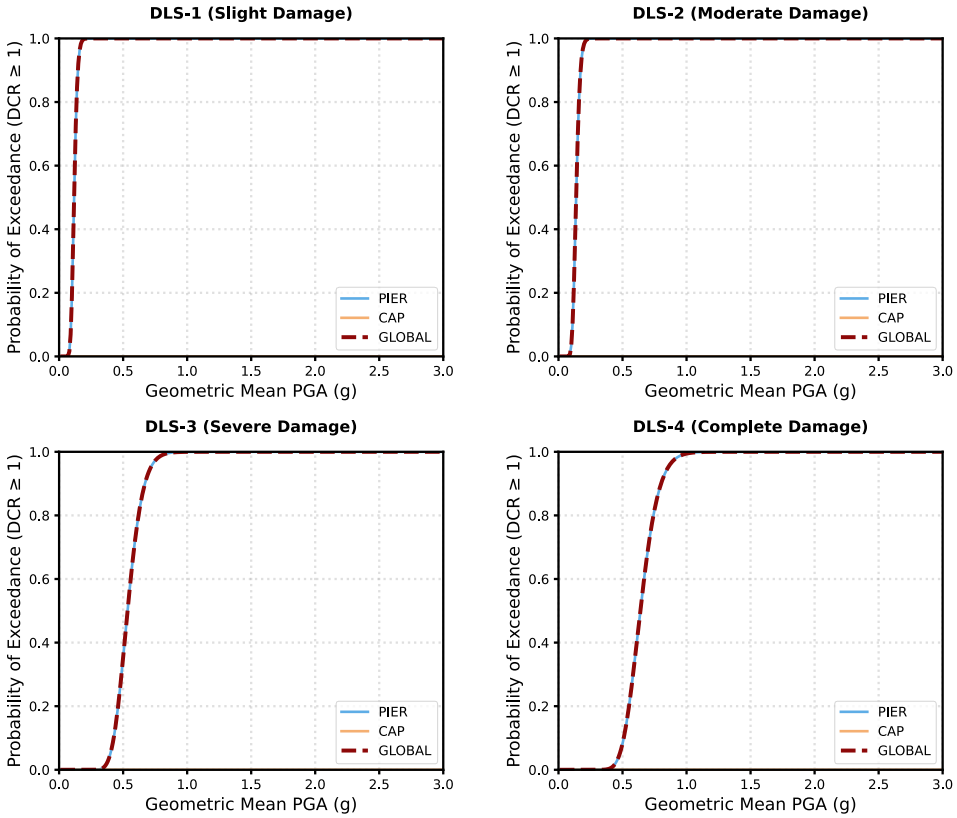

Figure C. 4. Component and System Fragility for the Fixed-Pier Bridge

iv) Fragility based on cloud analysis for the global Case 2 (Friction Orthogonal (0°))

The Figure C. 5. presents the cloud-based assessment of the fragility of the friction orthogonal (0°) bridge configuration. Regression analysis based on the Demand Capacity Ratio (DCR) to Peak Ground Acceleration (PGA) for components and systems. The resulting fragility curves will quantify the probability of exceedance and define the global seismic vulnerability of the bearing-supported bridge, as shown in Figure C. 6.

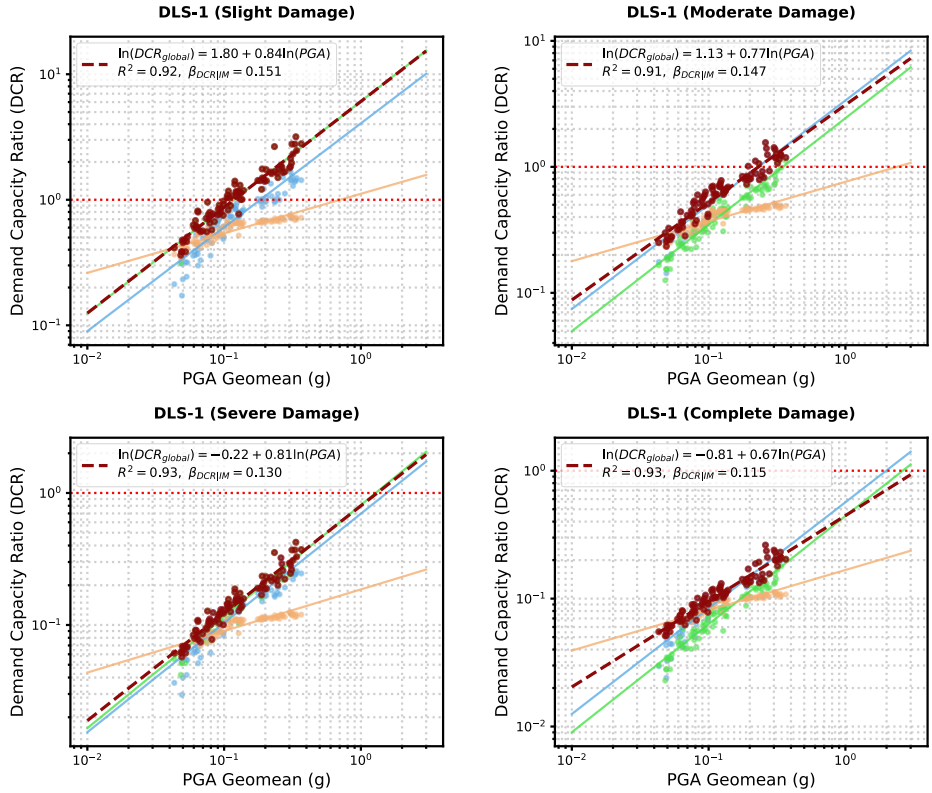

Figure C. 5. Regression-based probabilistic seismic (DCR) against (PGA_{geo}) analysis for component and the global friction orthogonal bridge

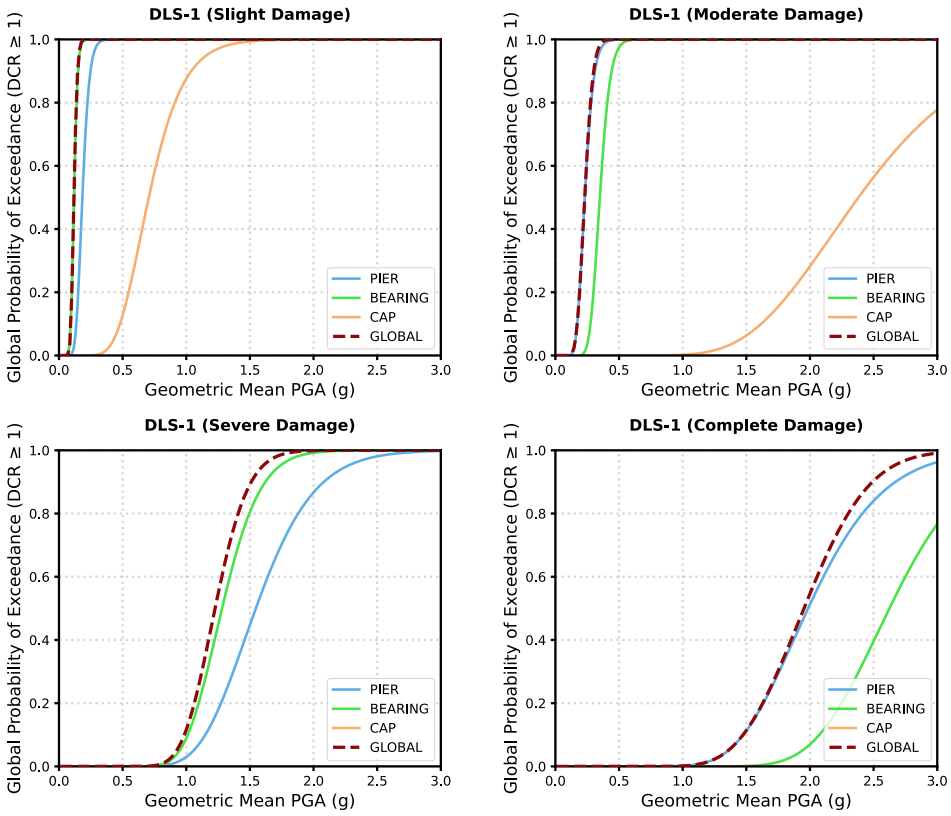

Figure C. 6. Component and System Fragility for the Friction Orthogonal (0°) Bridge

v) Fragility based on cloud analysis for the global Case 3 (Friction Skew (30°))

As with the previous analysis, this Figure C. 7. discusses the cloud-based fragility analysis for the friction-skewed (30°) bridge configuration. Regression analysis is used to define the probabilistic relationship between the Demand Capacity Ratio (DCR) and PGA_{geo} for each component and for the entire system. The resulting fragility curves for each component and for the entire system quantify the seismic vulnerability of the skewed friction-supported bridge in Figure C. 8.

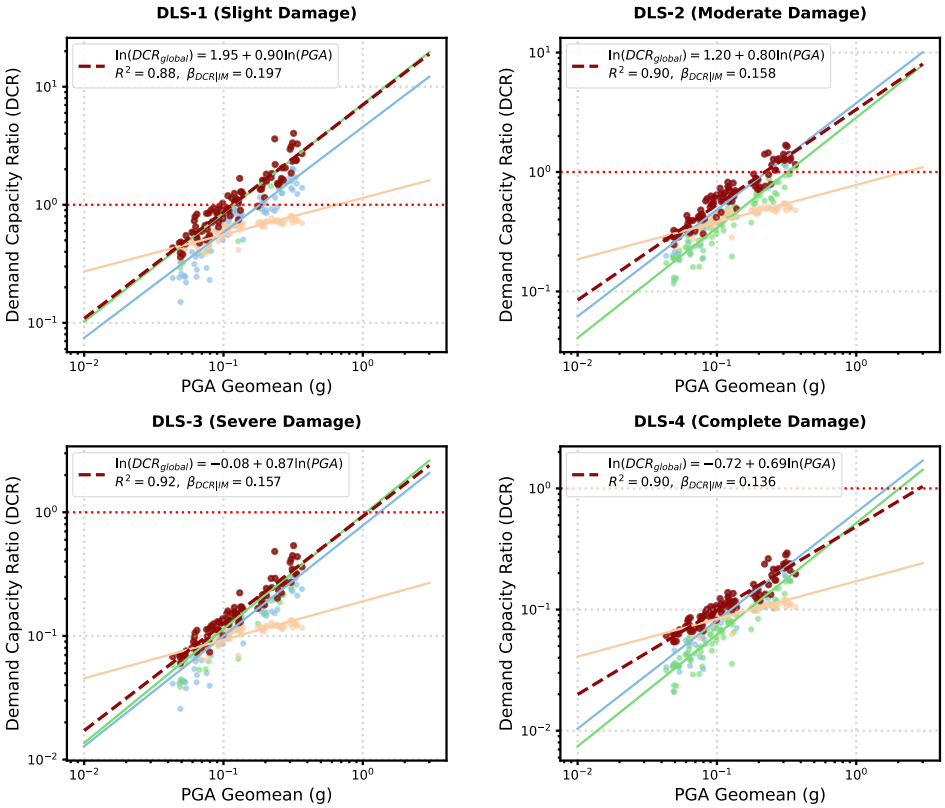

Figure C. 7. Regression-based probabilistic seismic (DCR) against (PGA_{geo}) analysis for companent and the global friction skew bridge

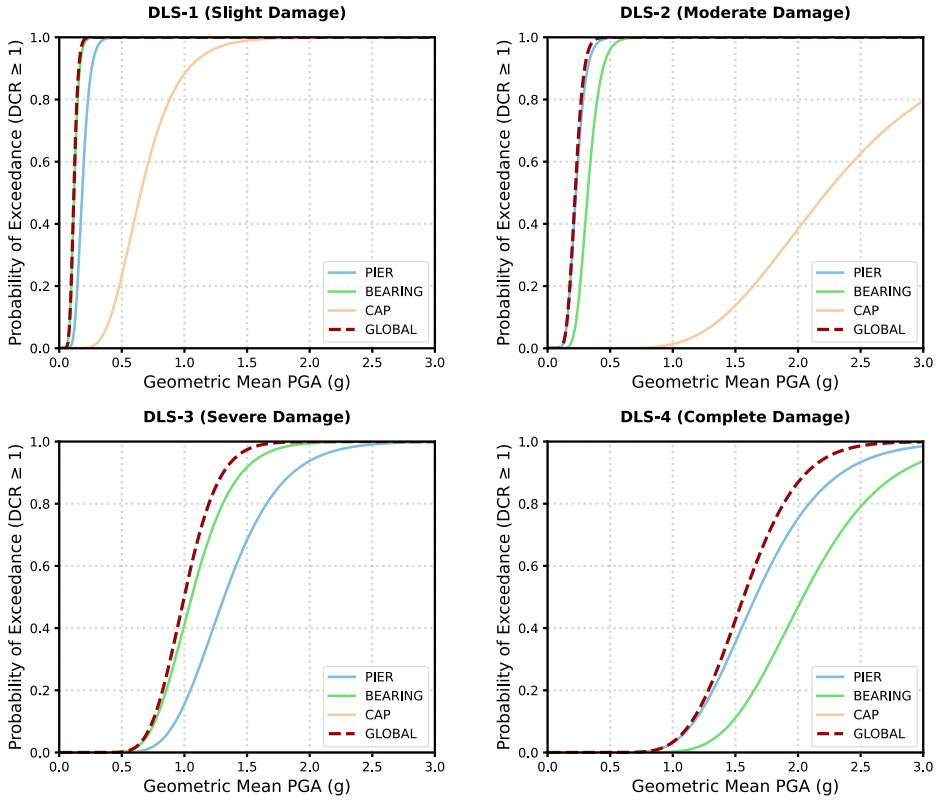

Figure C. 8. Component and System Fragility for the Friction Skew (30°) Bridge

APPENDIX D. Component and Global Fragility Parameters

i) Fragility parameters for the component and the global system of Case 1

The fragility analysis for the fixed base case is dominated by the capacities of the pier columns. This is evident from the fact that the median capacity θ and dispersion β values of piers and the global system are identical. The T-cap beam

has been determined to have the greatest level of structural integrity; therefore, the T-cap is eliminated from the hierarchy based upon its large median capacity of θ. Lacking a mechanism for seismic isolation, the rigid load path places all load on the pier, which reaches its ultimate damage state at a median PGA of 0.6389 g, as shown in Table D. 1.

Table D. 1 Fragility Parameters for Structural Components and Global System (Fixed Case)

Damage State	Component	Max DCR	θ (Median)	β (Dispersion)	R^2
Slight (DLS-1)	PIER	2.783	0.1169g	0.1765	0.921
	CAP	0.377	397.493g	0.3937	0.702
	GLOBAL	**2.783**	**0.1169g**	**0.1765**	**0.921**
Moderate (DLS-2)	PIER	2.304	0.1376g	0.1765	0.921
	CAP	0.257	4233.883g	0.3937	0.702
	GLOBAL	**2.304**	**0.1376g**	**0.1765**	**0.921**
Severe (DLS-3)	PIER	0.477	0.5346g	0.1765	0.921
	CAP	0.063	2.55 * 10^7g	0.3937	0.702
	GLOBAL	**0.477**	**0.5346g**	**0.1765**	**0.921**
Complete (DLS-4)	PIER	0.388	0.6389g	0.1765	0.921
	CAP	0.057	4.88 * 10^7g	0.3937	0.702
	GLOBAL	**0.388**	**0.6389g**	**0.1765**	**0.921**

ii) Fragility parameters for the component and the global system of Case 2 (Friction Orthogonal (0°))

The employment of unreinforced elastomeric pad bearings in an orthogonal configuration (Case 2) results in a different seismic demand pattern compared to the fixed-base configuration. In the slight damage, global fragility is controlled by the bearings (θ = 0.1181g), which act as a structural fuse. As seismic demands increase, the pier becomes the governing component for the moderate and complete damage states. However, it is noteworthy that the isolation effect provided by the bearings significantly improves the pier's seismic resilience by increasing its median capacity from 0.6389g to 1.9855g. while the cap beam is structurally overdesigned, as shown in Table D. 2.

Table D. 2 Fragility Parameters for Structural Components and Global System (case 2)

Damage State	Component	Max DCR	θ (Median)	β (Dispersion)	R^2
Slight (DLS-1)	PIER	1.881	0.1838g	0.2314	0.872
	BEARING	3.176	0.1181g	0.1837	0.915
	CAP BEAM	0.749	0.7057g	0.302	0.8
	GLOBAL	**3.176**	**0.1177g**	**0.1796**	**0.919**
Moderate (DLS-2)	PIER	1.558	0.2308g	0.2314	0.872
	BEARING	1.271	0.3491g	0.1837	0.915
	CAP BEAM	0.51	2.3806g	0.302	0.8
	GLOBAL	**1.558**	**0.2301g**	**0.19**	**0.91**
Severe (DLS-3)	PIER	0.323	1.5465g	0.2314	0.872
	BEARING	0.424	1.2809g	0.1837	0.915
	CAP BEAM	0.125	208.483g	0.302	0.8
	GLOBAL	**0.424**	**1.2263g**	**0.1598**	**0.934**
Complete (DLS-4)	PIER	0.262	1.9855g	0.2314	0.872
	BEARING	0.231	2.6242g	0.1837	0.915
	CAP BEAM	0.112	291.300g	0.302	0.8
	GLOBAL	**0.262**	**1.9530g**	**0.1715**	**0.925**

iii) Fragility parameters for the component and the global system of Case 3 (Friction skew (30°))

Fragility analysis of the skew bridge (30°) in Case 3 shows seismic behaviour affected by geometric irregularity. Ground motion affects the bearings, increasing the bridge's sensitivity to a global "minor" level of damage (θ = 0.1160 g), a consistent feature of these bearings' role as sacrificial components. By adding a skew angle, the demand dispersion (β) becomes larger, and the average capacity at higher intensity levels becomes smaller than the response to the orthogonal layout. The global average capacity is reduced by about 15% for "full" damage, from 3.3401 g (Case 2) to 2.8384 g - indicating that the bridge axis rotation will accelerate the rate of pier and bearing damage, as shown in Table D. 3.

Table D. 3 Fragility Parameters for Structural Components and Global System (skew case)

Damage State	Component	Max DCR	θ (Median)	β (Dispersion)	R^2
Slight (DLS-1)	PIER	2.027	0.1828g	0.272	0.831
	BEARING	4.03	0.1187g	0.2519	0.852
	CAP BEAM	0.804	0.6508g	0.3615	0.736
	GLOBAL	**4.03**	**0.1168g**	**0.218**	**0.885**
Moderate (DLS-2)	PIER	1.678	0.2258g	0.272	0.831
	BEARING	1.612	0.3208g	0.2519	0.852
	CAP BEAM	0.548	2.2255g	0.3615	0.736
	GLOBAL	**1.678**	**0.2203g**	**0.1976**	**0.903**
Severe (DLS-3)	PIER	0.348	1.3171g	0.272	0.831
	BEARING	0.537	1.0567g	0.2519	0.852
	CAP BEAM	0.134	204.9055g	0.3615	0.736
	GLOBAL	**0.537**	**0.9974g**	**0.1815**	**0.917**
Complete (DLS-4)	PIER	0.283	1.6605g	0.272	0.831
	BEARING	0.293	2.0397g	0.2519	0.852
	CAP BEAM	0.121	287.3749g	0.3615	0.736
	GLOBAL	**0.293**	**1.5652g**	**0.1956**	**0.905**

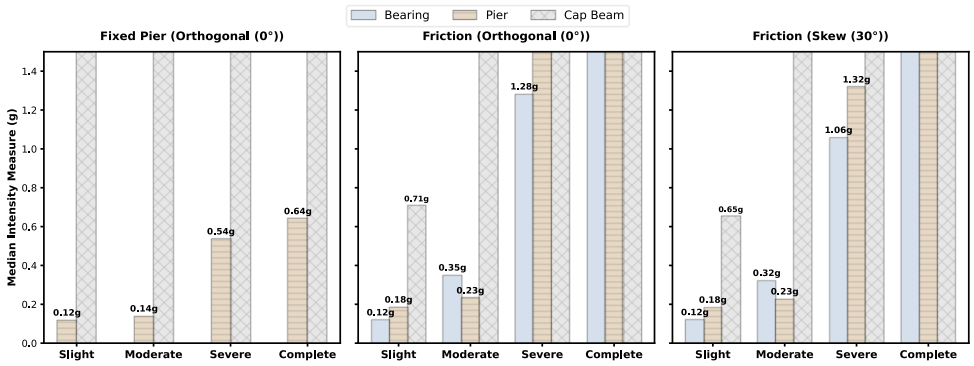

Figure C. 9 Comparing the median intensity_g of all components across the three cases